ISTANBUL TECHNICAL UNIVERSITY ★ GRADUATE SCHOOL OF SCIENCE ENGINEERING AND TECHNOLOGY

PERFORMANCE OF IEEE 802.15.4a BASED UWB SYSTEMS IN THE PRESENCE OF LICENSED SYSTEMS

M.Sc. THESIS

Çağlar FINDIKLI

Department of Electronics & Communication Engineering

Telecommunication Engineering Programme

JUNE 2012

ISTANBUL TECHNICAL UNIVERSITY ★ GRADUATE SCHOOL OF SCIENCE ENGINEERING AND TECHNOLOGY

PERFORMANCE OF IEEE 802.15.4a BASED UWB SYSTEMS IN THE PRESENCE OF LICENSED SYSTEMS

M.Sc. THESIS

Çağlar FINDIKLI
(504091356)

Department of Electronics & Communication Engineering

Telecommunication Engineering Programme

Thesis Advisor: Prof. Dr. Mehmet Ertuğrul ÇELEBİ

JUNE 2012

İSTANBUL TEKNİK ÜNİVERSİTESİ ★ FEN BİLİMLERİ ENSTİTÜSÜ

LİSANSLI SİSTEMLERİN VARLIĞINDA IEEE 802.15.4a TABANLI ULTRA GENİŞ BANTLI SİSTEMLERİN BAŞARIMI

YÜKSEK LİSANS TEZİ

Çağlar FINDIKLI
(504091356)

Elektronik ve Haberleşme Mühendisliği Anabilim Dalı

Telekomünikasyon Mühendisliği Programı

Tez Danışmanı: Prof. Dr. Mehmet Ertuğrul ÇELEBİ

HAZİRAN 2012

Çağlar FINDIKLI, a **M.Sc.** student of ITU **Institute of / Graduate School of Science Engineering and Technology** student ID **504091356**, successfully defended the **thesis/dissertation** entitled "**PERFORMANCE OF IEEE 802.15.4a BASED UWB SYSTEMS IN THE PRESENCE OF LICENSED SYSTEMS.**", which he prepared after fulfilling the requirements specified in the associated legislations, before the jury whose signatures are below.

Thesis Advisor : Prof. Dr. Mehmet Ertuğrul ÇELEBİ ....
İstanbul Technical University

Jury Members : Prof. Dr. Ümit AYGÖLÜ ....
İstanbul Technical University

Yard. Doç. Dr. Serhat ERKÜÇÜK ....
Kadir Has University

Date of Submission : 4 May 2012
Date of Defense : 8 June 2012

To memory of my grandmother Meliha FINDIKLI,

FOREWORD

I initially would like to thank my supervisor Prof. Dr. Mehmet Ertuğrul Çelebi for his guidance, advice and criticism throughout the thesis.

I would also like to thank Assist. Prof. Dr. Serhat Erküçük of Kadir Has University for his suggestions and comments on my research work. Part of the work in this thesis has resulted from my contribution to his 7th European Framework Programme project. Hence, I also would like to acknowledge the Marie Curie International Reintegration Grant within the 7th European Community Framework Programme for providing me financial support.

I finally would like to express my profound appreciation to my family for their continuous support.

May 2012

Çağlar FINDIKLI
Engineer

TABLE OF CONTENTS

Page

ABBREVIATIONS

A-Rake : All-Rake
BPPM : Binary Pulse Position Modulation
BPSK : Binary Phase Shift Keying
BER : Bit Error Rate
CM : Channel Model
dBm : Decibel Miliwatt
DARPA : Defense Advanced Research Projects Agency
DECT : Digital Enhanced Cordless Telephone
ECMA : European Computer Manufacturers Association
FCC : Federal Communications Commission
FIR : Finite Impulse Response
GHz : Gigahertz
GPS : Global Positioning System
GSM : Global System for Mobile
IEEE : Institute of Electrical and Electronics Engineers
IEEE-SA : IEEE Standard Association
ITU-R : International Telecommunication Union Radiocommunication
LAN : Local Area Network
LOS : Line of Sight
MAN : Metropolitan Area Network
Mbps : Megabits per second
MHz : Megahertz
nW : Nanowatt
NLOS : Non Line of Sight
OFDM : Orthogonal Frequency Division Multiplexing
P-Rake : Partial-Rake
SIR : Signal-to-Interference Ratio
SNR : Signal-to-Noise Ratio
S-Rake : Selective-Rake
TDMA : Time Division Multiple Access
TG : Task Group
TH : Time Hopping
UMTS : Universal Mobile Telecommunication System
UWB : Ultra-Wideband
WIMAX : Worldwide Interoperability for Microwave Access
WPAN : Wireless Personal Area Network

LIST OF FIGURES

Page

PERFORMANCE OF IEEE 802.15.4a BASED UWB SYSTEMS IN THE PRESENCE OF LICENSED SYSTEMS

SUMMARY

In recent years, spectrum sharing techniques have drawn great amount of interest due to lacking frequency bands for licensed radio systems. UWB technology is one of the emerging spectrum sharing techniques that can communicate at very low power spectral density levels using a large portion of the electromagnetic spectrum. UWB systems transmit in a way that they do not interfere much with licensed systems in the same frequency band.

Despite the low transmission power of UWB systems, an important research topic in the UWB communications technology is the *coexistence of UWB systems with licensed systems* that already exist or are expected to exist in future standards. Accordingly, regulatory agencies in Europe and Japan have made the implementation of detect-and-avoid techniques mandatory in some bands to avoid interference to existing systems. Hence, the emission power of UWB system should be reduced or the UWB communication should be stopped when the UWB transceivers are located near the terminal of the primary systems. However, the latter option is inconvenient for the UWB systems which will slow down the transmission data rate. As for the first option, the UWB impulse radio based Wireless Personal Area Network standard IEEE 802.15.4a has suggested using a linear combination of pulses to reduce interference to coexisting primary systems.

In this thesis, the implementation of various linear combinations of pulses are considered for a harmonious coexistence, and the UWB impulse radio system performance is assessed in the presence of active narrowband or wideband licensed systems. For that, possible transmitter and receiver structures are studied and adapted for the physical layer of the IEEE 802.15.4a standard.

The study shows that while BER performance of coherent and noncoherent receiving structures may be slightly degraded with the use of linear combination of pulses when there is no active primary system, the performances can be significantly improved with appropriate filtering techniques at the receiver when the primary system is active. Moreover, the selection of various pulse types for different types of licensed systems is presented for practical considerations. The results are important for the implementation of the IEEE 802.15.4a based UWB systems coexisting with licensed systems.

LİSANSLI SISTEMLERİN VARLIĞINDA IEEE 802.15.4a TABANLI ULTRA GENİŞ BANTLI SİSTEMLERİN BAŞARIMI

ÖZET

Spektrum paylaşım teknikleri, son yıllarda elektromanyetik spektrumdaki kalabalıklaşma ve kullanıma müsait frekansların etkin kullanılması gerekliliğinden oldukça ilgi çekmiştir. Spektrum paylaşım tekniklerinden biri olan Ultra Geniş Bantlı sistemler, elektromanyetik spektrumun büyük bir bölümünü aynı frekans bandındaki lisanslı dar bantlı sistemleri büyük ölçüde etkilemeden iletim yapabilecek şekilde tasarlanmış ve dünya çapında gelişmekte olan telsiz iletişim teknolojisidir.

Ultra Geniş Bant uygulamaları askeri, arama-kurtarma, iç güvenlik, otomotiv ve medikal alanlarındaki duvar içi-arkası ve zemin görüntülemesi, hedef sensör veri toplanması ve takibi, hassas mesafe tayini, sınır ihlal tespiti, kalp atış ve soluk alış-veriş hızı tespiti ve kestirimi, çarpışma önleme, yol yardımcısı, envanter takibi ve kimlik saptama gibi geleneksel radar, yer tespiti ve telsiz iletişim uygulamalarını kapsar.

Ultra Geniş Bant teknolojisini, bahsedilen uygulamalar ve alanlar için cazip bir seçenek haline getiren, geniş lisanssız bant genişliği, elektromanyetik spektrum paylaşımına olanak sağlayan düşük spektral güç yoğunluğu, büyük kanal kapasitesi, düşük işaret gürültü oranlarında çalışabilme, yüksek çok yol çözünürlülüğü, düşük olasılıkta tespit ve yakalanma, karışmaya karşı direnç, üstün malzeme nüfuz yeneteği, çoklu erişim yetkinliği, basit alıcı verici mimarisi vb. özelliklerdir.

Ultra Geniş Bantlı sistemlerin düşük iletim gücüne rağmen, bu cihazların mevcut ve gelecekteki standardlarla birlikte varolabilirliği Ultra Geniş Bantlı iletişim teknolojisindeki önemli bir konu başlığıdır. Bunun sonucunda, Ultra Geniş Bantlı sistemlerin düşük iletim gücüne rağmen, Avrupa ve Japonya'daki spektrum düzenleme kurulları mevcut sistemlere olan girişimleri engellemek için algıla-ve-kaçın tekniklerinin ortak kullanılan frekans bantlarında gerçekleştirilmesini zorunlu kılmıştır. UWB dürtü radyoları üzerine kurulu olan ve geçtiğimiz yıllarda onaylanan IEEE 802.15.4a standardı bu durumla ilgili tavsiyelerde bulunmaktadır. Bunlardan bazıları ortak kullanılan iletim bandı yerine başka bir bant kullanılması, eğer ortak bant kullanılacaksa iletimin geciktirilmesi veya istenilen frekanslarda ani düşüş sağlayabilmek için darbelerin doğrusal bileşimini kullanmak olarak özetlenebilir. Bu tavsiyeleri değerlendirilecek olursa, düşük maliyetli UWB dürtü radyolarında bant değiştirmek masraflı olabilir. Diğer taraftan ortak bantta oldukça aktif bir birincil sistem olması durumunda UWB sisteminin iletimini geciktirmesi sonucu iletim hızı oldukça yavaşlayabilir.

Lisanslı sistemlere girişim yaratmaktan kaçınmak**,** literatürde darbe tasarım teknikleri ile sağlanmaya çalışılmıştır. Şu ana kadarki darbe tasarım teknikleri iki ana konu

üzerine yoğunlaşmıştır. Bunlardan birincisi iletişim için izin verilen spektrum maskesinde darbe spektrumunun optimizasyonu, ikincisi ise dar bantlı girişimlerin olduğu frekanslarda ani düşüş sağlamaktır. Bunun için sonlu dürtü yanıtlı süzgeç tasarımı, özel fonksiyonların (örneğin, Hermite fonksiyonları) özfonksiyon nitelikleri veya kod sözcüğü tasarım teknikleri kullanılmıştır. Bu tür çalışmaların ortak özelliği, hem spektrum optimizasyonu için, hem de istenilen frekansta ani düşüş yaratabilmek için çok sayıda katsayı kullanmalarıdır. Diğer taraftan IEEE 802.15.4a standardına göre, darbelerin doğrusal birleşimi kullanılarak elde edilecek frekanstaki ani düşüşler için en fazla 4 katsayı kullanılmalıdır. Bu da süzgeç tasarımı için az sayıda katsayı kullanılmasına denk gelmektedir. IEEE 802.15.4a standardı tarafından öngörülen kısıtları dikkate alarak ve z-dönüşümünden yararlanarak, az sayıda katsayı ile istenilen frekans değerlerinde ani düşüş sağlayabilen darbelerin doğrusal birleşimi tekniğini kullanılmıştır. Buna göre yeterince katsayı kullanılmaması yüzünden, elde edilen spektrumda birden çok ani düşüş sağlanamayacağı ve spektrum maskesinin iyi bir şekilde kullanılamayacağı gözlenilmiştir. Her ne kadar bu tür yöntemlerle lisanslı sistemlere olan girişim azaltılsa da, yeni darbelerin kullanıldığı durumda ikincil Ultra Geniş Bant sistemlerin başarımını da gözlemlemek önemlidir.

Literatürde lisanslı sistemlere girişim yaratmamak için yapılan darbe tasarımı çalışmalarında, genel olarak istenilen spektrum maskesinin iyi bir şekilde kullanılıp kullanılmadığı veya istenilen frekansta ani düşüş sağlanıp sağlanmadığı çalışılmış, ancak yeni darbelerle olan sistem başarımı üzerinde yeterince durulmamıştır. Diğer taraftan lisanslı sistemlerin Ultra Geniş Bant sistemlere olan etkileri literatürde incelenmiştir. Bu çalışmalarda, gerek bazı lisanslı sistemlerin (GSM, UMTS, WiMAX), gerekse de dar-bantlı sistemlerle kullanılan bazı modülasyonların Ultra Geniş Bant sistemlerle etkileşimleri incelenmiş, alıcı antene lisanslı sistemin bandını geçirmeyen bir süzgeç konulduğunda Ultra Geniş Bant sistemin başarım iyileşmesi üzerine çalışılmıştır. Her ne kadar lisanslı dar bantlı sistemlerin Ultra Geniş Bant sistemlerle etkileşimini incelemek önemli olsa da, bu çalışmayı yeni tasarlanmış girişim azaltan darbe şekilleriyle ve IEEE 802.15.4a standardına uygun bir biçimde gerçekleştirmek önemlidir. Ancak bu konu literatürde henüz incelenmemiştir. Bununla ilgili literatürde eksikliğini görülen konular şöyle özetlenebilir:

i) Avrupa ve Japonya spektrum düzenleme komisyonu kararına ve IEEE 802.15.4a standardına uygun bir şekilde, yani normal iletim gücünü istenilen frekansta düşürmek için az sayıda katsayı ile oluşturulan yeni darbelerin sistem başarımının dar- ve geniş-bantlı lisanslı sistemler tarafından nasıl etkilendiğini incelenmesi gerekir.

ii) Standarda uygun evre-uyumlu ve evre-uyumsuz alıcı yapılarının sistem başarımına etkilerini incelenmesi gerekir.

Ultra Geniş Bantlı sistemler için kaçınma konusunda literatürde henüz yeterince incelenmemiş olan IEEE 802.15.4a standardı gerçekleştirimine uygun araştırmalar yürütülmelidir.

Bu tezin esas amacı, literatürdeki belirtilen eksiklerden hareketle, dar veya geniş bantlı girişim olduğunda IEEE 802.15.4a standardının fiziksel katmanının gerçeklenmesi ve sistem başarımının ölçülmesidir. Dolayısıyla, istenilen frekanslarda ani düşüşler elde etmek için IEEE 802.15.4a standardında önerilen çeşitli darbelerin doğrusal birleşimi kullanılmasıdır. Ayrıca, dar bantlı girişim daha ileri seviyede bastıracak evre uyumlu ve evre uyumsuz alıcı yapıları sunmaktır. Bunun sonucunda IEEE 802.15.4a sistemin başarımını değişik senaryolar altında sınamaktır. Bu senaryolar alıcı verici yapısının, girişim seviyesinin, girişim tipinin (değişken bant genişliğinin ve alt taşıyıcı sayısı), IEEE 802.15.4a standardındaki ve önerilen darbelerin doğrusal birleşimi tiplerinin ve evre uyumlu ve evre uyumsuz alıcılar için IEEE 802.15.4a kanal modelleridir. Bu çalışmanın sonuçları, düzenleyici kurumların birlikte varolabilirlik için konulanan kurallarına uyarken aynı zamanda makul bir sistem başarımına ulaşan IEEE 802.15.4a sisteminin alternatif olarak gerçeklenmesi için önemlidir.

Bu tezde, IEEE 802.15.4a tabanlı Ultra Geniş Bantlı sistemlerin dar ve geniş bantlı girişime sebep olan lisanslı sistemlerle aynı frekans bandında çalışması için darbelerin doğrusal birleşimi ve ilişkin evre uyumlu ve evre uyumsuz alıcı yapılarının gerçeklenmesi araştırılmıştır. Bunun sonucunda, değişik darbelerin doğrusal birleşimini kullanan ve birlikte varolabilirliğe imkan veren uyarlanmış alıcı verici yapısına sahip sistemin başarımı IEEE 802.15.4a standardı doğrultusunda gerçeklenen sistemle karşılaştırılmıştır. Bunlara ek olarak, değişik tipteki lisanslı sistemler için darbelerin çeşitli doğrusal birleşimleri pratik senaryolar için göz önüne alınmıştır. Çalışmanın sonuçları darbelerin doğrusal birleşimi kullanıldığında ve aktif bir girişime neden olan dar-bantlı lisanslı sistem yokken, evre uyumlu ve evre uyumsuz alıcı yapılarının Bit Hata Oranı başarımlarını biraz kötüleştirirken, buna karşın aktif tek veya çoklu girişime neden olan lisanslı sistemin olduğu durumda Bit Hata Oranı alıcıdaki ön filtrelemeyle belirgin bir ölçüde iyileştirilebileceğini göstermiştir.

Dahası, geniş bantlı girişimin olduğu yerde, geniş ani düşüş ve daha etkin spektrum şekillendirmesinden dolayı yüksek dereceli darbelerin (örneğin lcp_2, lcp_3) doğrusal birleşimi kullanılması sistem başarımı daha iyi bir şekilde tazmin edebilmektedir. Bunların yanında, sabit alt taşıyıcı sayısı için artan bant genişliğinde Bit Hata Oranı azalma eğiliminde olduğu görülmüştür. Buradan, Ultra Geniş Bantlı sisteminin daha geniş ve çok sayıda alt taşıyıcı sayısına sahip WiMAX sitemlerle en uyumlu biçimde birlikte varolabileceği kanısına varılmıştır.

Bu çalışmanın sonuçları, uyarlanmış alıcı-verici yapılarının Avrupa ve Japonya’daki düzenleyici kurumların talimatlarına uyarken aynı zamanda makul bir sistem başarımına ulaşması açısından oldukça önemlidir.

1. INTRODUCTION

1.1 Overview of UWB

In recent years, spectrum sharing techniques have drawn great amount of interest due to lacking frequency bands for licensed radio systems. Ultra-Wideband (UWB) technology is one of the emerging spectrum sharing techniques that can communicate at very low power spectral density levels using a large portion of the electromagnetic spectrum. UWB systems transmit in a way that they do not interfere much with licensed systems in the same frequency band [1]. This technology spans the coverage of wireless personal area networks for data communications as a particularly appealing transmission technique for applications requiring either high bit rates (above 100 Mbps) over short ranges (around 10m) or low bit rates (typically around 1 Mbps) over medium-to-long ranges (up to 100m) [2]. UWB also inherits conventional radar and localization applications in the areas of military, search and rescue, law enforcement, automotive and medical such as through and –in wall/ground imaging, target sensor data collection, tracking, precision location, intrusion detection, vital sign monitoring (heart beat and respiration rate detection and estimation), collision avoidance, roadside assistance, inventory tracking and personal identification etc. [3-6].

The UWB technology offers some unique qualities such as wide unlicensed bandwidth, low power spectral density that allows it to share the frequency spectrum, large channel capacity, ability to work with low SNR ratio, high multipath resolution, low probability of intercept and detection, resistance to jamming, superior material penetrating capability, multiple access capability and simple transceiver architecture, which make these systems an attractive choice for the above mentioned applications and fields.

The history of ultra wideband communications roots back in the early days of radio. In the 1900s, Marconi spark gap transmitter communicated by spreading a signal over a very wide bandwidth [7]. This way of occupying the spectrum did not allow for sharing. Therefore, the communications agencies abandoned wideband communication in favor of narrowband or tuned communication, in which the FCC governed spectrum allocation.

Approximately fifty years after Marconi, modern pulse-based transmission gained momentum in military applications in the form of impulse radars [8]. Some of the pioneers of modern UWB communications in the United States from the late 1960's are Henning Harmuth of Catholic University of America and Gerald Ross and K. W. Robins of Sperry Rand Corporation. From the 1960's to the 1990's, this technology was restricted to military and Department of Defense applications under classified programs such as highly secure and covert communications and radar applications [7]. However, the advancement in microprocessing and fast switching in semiconductor technology has made UWB ready for commercial applications. Beginning in the late 1980's, small companies specializing in basic UWB started basic research and development on communications and positioning system.

As interest in the commercialization of UWB has increased over the past several years, developers of UWB systems began pressuring the FCC to approve UWB for commercial use. In April 2002, after extensive commentary from industry the FCC issued first report and authorized the unlicensed use of UWB in the range of 3.1 to 10.6 GHz for communications [9]. Each radio channel can have a bandwidth of more than 500 MHz, depending on its center frequency. The FCC power spectral density emission limit for UWB emitters operating in the UWB band is -41.3 dBm/MHz (75 nW/MHz) to ensure that UWB devices do not cause harmful interference to licensed services and other important radio operations. This is the same limit that applies to unintentional emitters such as televisions and computer monitors in the UWB band, the so called Part 15 limit providing regulations to support deployment of UWB radio systems. However, the emission limit for UWB emitters can be significantly lower (as low as -75 dBm/MHz) in other segments of the spectrum. The FCC regulations classify UWB applications into three categories which are communications, imaging, and vehicular radar with different emission regulations in each case. The spectral mask assigned by FCC for indoor UWB communication systems is shown in Fig 1.1. The spectral mask for outdoor devices is 10 dB lower than that for indoor devices between 1.61 GHz and 3.1 GHz.

According to FCC regulation [9], indoor UWB devices must consist of handheld equipment, and their activities should be restricted to peer-to-peer operations inside buildings.

The FCC's rule dictates that no fixed infrastructure can be used for UWB communications in outdoor environments. Therefore, outdoor UWB communications are restricted to handheld devices that can send information only to their associated receivers.

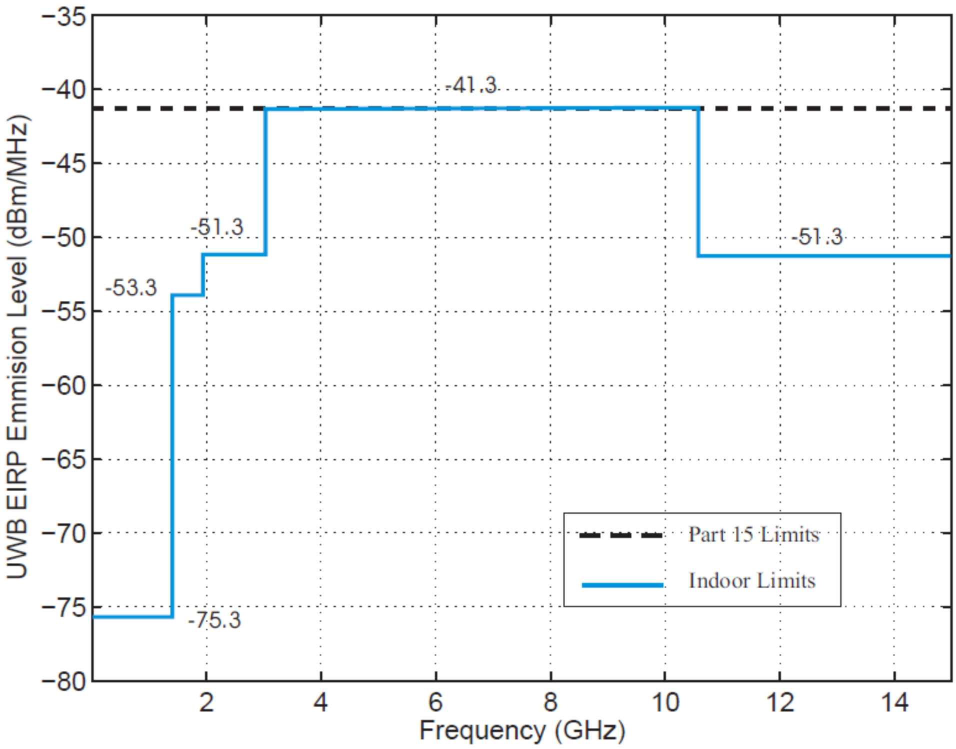

Figure 1.1 : FCC allocated spectral mask for indoor UWB systems [9].

In 1991, DARPA defined the standard for a signal to be classified as UWB as electromagnetic signal waveforms that have an instantaneous fractional bandwidth greater than 25% [7]. This definition is common approach in radar applications. However, in communications perspective, FCC and ITU-R [9], UWB is defined in terms of a transmission from an antenna for which the emitted signal instantaneous bandwidth exceeds 500 MHz or a fractional bandwidth of more than 20%. The fractional bandwidth defined as

$$f_{BW} = \frac{f_H - f_L}{f_c} \quad \textbf{(1.1)}$$

where f_C is carrier frequency written as

$$f_C = \frac{f_H + f_L}{2} \quad \textbf{(1.2)}$$

with f_H being the upper frequency of the -10 dB emission point, and f_L the lower frequency of the -10 dB emission point, as shown in the Figure 1.2.

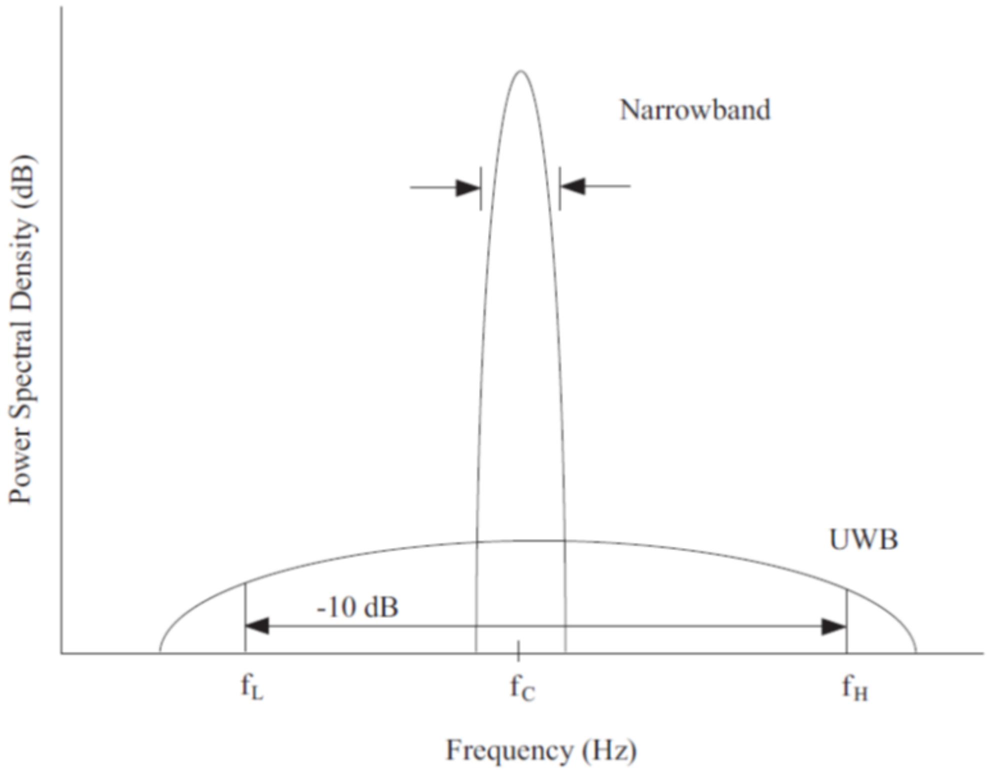

Figure 1.2 : Comparison of fractional bandwidth of a narrowband and UWB communication system [6].

UWB standardization efforts gained momentum after the publication of FCC report [11]. As a result of these efforts, Task Group (TG3a) was created to investigate physical layer alternatives for high date rate WPAN systems (i.e., 802.15.3 physical layer).

In December 2002, TG3a established technical requirements and selection criteria for a wireless personal area and reviewed proposals by different companies such as Time Domain, Intel, Texas Instruments, XtremeSpectrum etc. This new standard would enable high date rate WPAN up to 480 Mbps over a broad range of applications including the wireless transmission of images and video. Two candidate technologies determined were are Multi-Band OFDM UWB and Direct Sequence UWB. TG3a fell apart because of a deadlock between supporters of two competing UWB technologies and was disbanded in 2006. Direct Sequence UWB, which was promoted by the ZigBee Alliance, joined in TG4a, while Multi-Band OFDM UWB was adopted by the WiMedia Alliance which published in another telecommunications standardization body ECMA as ECMA-368 [12].

On the other side of these efforts, low rate alternative physical layer TG4a was created in March 2004 with the goal of defining alternative physical layers able to provide the desired high precision ranging capability (1 m accuracy or better), and correspondingly high aggregate throughput and ultra-low power consumption (typically under -10 dBm) as well as adding scalability to data rates, longer range and lower cost [13].

In March 2005 a baseline specification was approved by the TG4a committee, consisting of two optional physical layers: UWB impulse radio (UWB-IR) and Chirp Spread Spectrum. While UWB-IR is operating in the three distinct bands (sub-gigahertz, low and high band) in the unlicensed UWB spectrum, Chirp Spread Spectrum is operating in the 2.4 GHz spectrum in industrial, scientific, and medical band which has nearly worldwide availability.

The committee completed the standardization of the IEEE 802.15.4a alternate physical layers in January 2007. In March of the same year, IEEE-SA Standards Board approved this standard as a new amendment to IEEE 802.15.4-2006. Therefore, IEEE 802.15.4a-2007 became the first international standard that specifies a wireless physical layer to enable precision ranging in order to support higher data rates, extended range, improved robustness against interference and mobility [14]. Furthermore, this standard enables new applications based on distance of the devices in a low-rate wireless personal area network.

For the implementation of UWB devices, the FCC is more relaxed compared to European and Japanese regulatory agencies. The European and Japanese counterparts are more concerned that UWB systems may cause interference to licensed systems. Hence, they require to implement detect-and-avoid techniques in same bands to avoid interference to coexisting systems [15].

Low duty cycle nature of UWB impulse radio based IEEE 802.15.4a is recognized by European regulation as an intrinsic detect-and-avoid technique, since the average power of the UWB over long time is reduced. However, they also rule out that the emission power of UWB system should be reduced or the UWB communication should be stopped when the UWB transceivers are located near the terminal of the primary systems. The latter option is inconvenient for the UWB systems as it reduces the time the UWB system can communicate. Hence, one of major implementation issues to be addressed in UWB communications has become the *coexistence of already existing or future licensed standards and UWB systems*.

Additional functions to share the spectrum cannot be added for the licensed systems, since these systems are assumed as primary systems and the specifications have already been fixed. Therefore, in the UWB system implementation, interference detect-and-avoid functions are needed to minimize the interference to primary systems.

1.2 Literature Review

In the coexistence literature, either UWB pulse design techniques or performance degradations of licensed and/or UWB systems have been studied.

In the pulse design techniques considered [16-18], codewords have been designed by employing delayed, weighted and summed version of Gaussian monocycle pulse to utilize the desired spectrum mask and suppress narrowband interference effectively with matched filtering. Also accurate spectrum shapes obtained using such as Butterworth, Chebyshev, elliptical at the expense of longer and more complex codeword usage to utilize the desired spectrum mask with no restriction on the number of filter coefficients [16]. In [17], authors suggested a digital FIR filter approach to synthesizing UWB pulses and proposed filter design techniques by which optimal waveforms that satisfy the spectral mask can be efficiently obtained. For a single pulse design, they develop a convex formulation for the design of the FIR filter coefficients that maximize the spectrum utilization efficiency in terms of both the bandwidth and power allowed by the spectral mask. For the orthogonal pulse design, a sequential strategy is derived to formulate the overall pulse design problem as a set of convex sub-problems which are then solved in a sequential manner to yield a set of mutually orthogonal pulses. As a result of these techniques, not only waveforms with high spectral mask compliance are provided but also simple modifications that can accommodate several other system objectives are permitted.

A method for the design of nonlinear phase, full-band, UWB pulses that satisfy the FCC's effective isotropic radiation power spectrum mask introduced in [18]. The method uses convex programming in each step of the iterative procedure that updates the phase distribution of the goal function. Due to its mathematical structure, this method can be easily modified in order to be applied, in sequential fashion, to several different orthogonal UWB pulse-design problems. This method produces a considerably larger number of orthogonal pulses with high energy compared to the methods introduced before. The problem of designing pulses which are orthogonal in reception is considered.

Later, a modification of this method is proposed that can be used to solve this problem. Authors also introduce statistical criteria of robustness of pulses' orthogonality in reception, to the variation of the pulses' shape caused by the channel transfer function. After that, a modification of the proposed method is presented that is capable of producing a set of pulses with predefined maximum value according to this criteria. It is shown that the proposed method can be used to efficiently design orthogonal pulses using a suboptimal value of the sample rate.

However, in the IEEE 802.15.4a standard, it is suggested to use linear combination of a few pulses, which is equivalent to using few filter coefficients, for obtaining notches and spectrum shaping purposes to reduce interference to coexisting primary systems.

Recently in [19], the authors considered possible implementations of linear combination of pulses as suggested in the standard, and studied the generated notches where the licensed system is located by conforming to restrictions in the standard and resulting code spectrum. Using the z-transform approach, it is shown that the number of these notches is limited and the notch locations are not flexible due to the limited number of pulses allowed by the standard.

In parallel to pulse design techniques, the effects of licensed systems on the UWB system performance (also referred to as interference from the UWB communications perspective) have been investigated [20-23]. In [20], jam resistance of UWB system with binary pulse position modulation utilizing rectangular pulses was investigated for interferences with various bandwidths. A simple approximation was obtained for the special case of tone interference. The jam resistance analysis was extended to more practical UWB waveforms such as Gaussian and Rayleigh monocycles. A comparison between the interference suppression capabilities of UWB and direct-sequence spread spectrum was carried out under conditions similar to both systems. The authors show that, the jam suppression of UWB is superior to that of direct-sequence spread-spectrum systems. In [21], effects of GSM900, UMTS and GPS systems on the UWB system performance (and vice versa) were studied. The authors evaluated and analyzed the performance of impulse radio based UWB systems employing differential binary phase keying modulation, differential-Rake receivers that does not require channel estimation and standardized IEEE 802.15.4a channel model in the presence of narrowband interference co-located in the same transmission band of the UWB signal [22]. The analysis was performed with and without frequency and timing synchronization errors, in order to identify the design constraints of the synchronization unit to guarantee the proper operation of the receiver over realistic propagation environments. The authors proposed an improved receiver structure for transmitted reference UWB systems to suppress both the narrowband interference and inter-pulse interference employed an FIR or IIR notch filter at the receiver and evaluated the improved system performance lower bound for UWB transmitted reference systems in [23].

The common approach in these studies is that the UWB systems employ pulses that do not take in to account the interference level caused by UWB systems to the licensed systems. However, as mandated by the European and Japanese regulatory agencies, the UWB systems should transmit pulses with reduced power levels at the frequency bands occupied by licensed systems.

1.3 Purpose of Thesis

Motivated by these condition, the major goal of this thesis is the implementation of the physical layer of the IEEE 802.15.4a standard in the presence of primary systems, i.e., interference from the UWB communications perspective. For that reason, various linearly combined pulses are used as suggested by the IEEE 802.15.4a standard that can generate notches at the desired frequencies. In addition, modified coherent and noncoherent receiver structures are presented that can suppress the interference effectively. Accordingly, UWB system performance is tested for various practical scenarios. These scenarios include studying the effects of the transmitter receiver structure, the interference level, interference type (various bandwidths and number of subcarriers), the pulse types (the pulse used in the IEEE 802.15.4a standard and proposed linearly combined pulses) and the IEEE 802.15.4a channel models for coherent and noncoherent receivers. The results of this study are important as they demonstrate an alternative implementation of the IEEE 802.15.4a system complying with the regulatory agency mandates for coexistence, and yet achieving a reasonable system performance.

1.4 Thesis Organization

The rest of the thesis is organized as follows. In Chapter 2, the physical layer of the IEEE 802.15.4a standard is presented. In Chapter 3, a modified transceiver structure that is suitable for coexistence is presented. In Chapter 4, simulation results are presented in order to assess the UWB system performance in the presence of a narrowband or a wideband interference for various scenarios. Concluding remarks are given in Chapter 5.

2. SYSTEM MODEL

In this chapter, the overview of IEEE 802.15.4a system model is presented. First, the transmit structure of the IEEE 802.15.4a based UWB impulse radios is presented in Section 2.1. Narrowband and wideband interference model is presented in Section 2.2. Then, the standardized IEEE 802.15.4a channel model is explained in Section 2.3. Finally, the conventional receiver structures for both coherent and noncoherent reception are introduced in Section 2.4.

2.1 Transmit Structure

The UWB impulse radio based IEEE 802.15.4a standard uses the combined binary phase shift keying / binary pulse position modulation for data transmission. While both the phase and position information can be detected by the coherent detection, only position information can be detected by noncoherent detection. The system model that supports both coherent and noncoherent data reception is explained as follows.

For reliable communications in a dense multipath environment, data transmission is achieved by burst of pulses. The power efficiency and correlation property of a specific pulse will influence the system performance. Therefore, it is important to select waveforms with high power efficiencies and good correlation properties so that the system performance can be enhanced.

It is common to use a Gaussian pulse due to easier generation and mathematical applicability. Various derivatives of Gaussian pulses are also used for generating pulses. The sixth derivative of Gaussian monocycle can be easily obtained, and its power efficiency is about 34.6%, which is the highest power efficiency of Gaussian monocycle and its derivatives [24].

Considering many candidates, the pulse shape selected for the IEEE 802.15.4a standard is given Figure 2.1. This pulse is a root-raised cosine pulse of 2ns duration, given as

$$p(t) = sinc\left(\pi\beta\frac{t}{T_c}\right)\frac{\cos\left(\pi\beta\frac{t}{T_c}\right)}{\left(1-\left(2\beta\frac{t}{T_c}\right)^2\right)}. \quad \textbf{(2.1)}$$

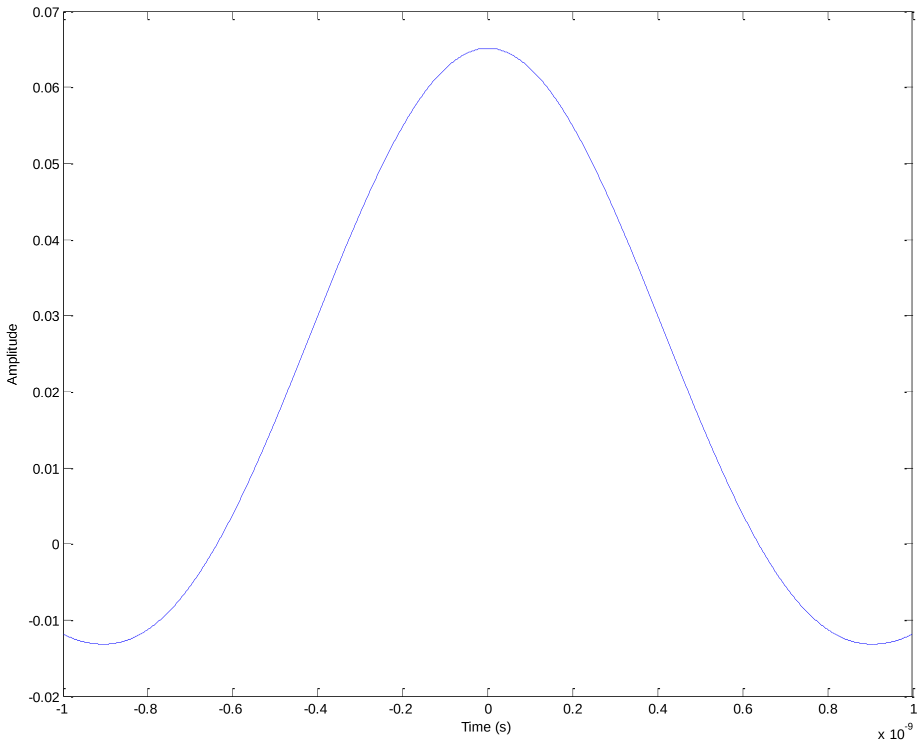

Figure 2.1 : UWB pulse used in IEEE 802.15.4a.

N_b pulses are transmitted consecutively, each within a chip time T_c = 2ns. Therefore, $T_b = N_b\ T_c$ is the burst duration. The symbol time $T_s = N_c\ T_c$, where N_c is the number of chips in a symbol, is much greater than the burst duration ($T_s \gg T_b$) in order to allow time hopping for multiple access and accommodate guard times to prevent intra- and inter-symbol interferences. With this symbol structure, the l^{th} symbol of the *1st* user that carries the position and phase information can be transmitted using the signal model

$$w_l^{(1)}(t) = \sum_{j=0}^{N_b-1} a_l^{(1)} s_j^{(1)} p\left(t - lT_s - jT_c - d_l^{(1)}\delta_p - c_l^{(1)}T_b\right) \quad \textbf{(2.2)}$$

where $w_l^{(1)}(t)$ is the waveform of the 1st user's l^{th} transmitted symbol consisting of N_b consecutive pulses, $p(t)$ is the transmitted pulse with duration $T_p \leq T_c$, where β is the roll-off factor and $s_j^{(1)} \in \{\pm1\}$ {j=0,1,…, N_b -1} is a scrambling sequence specific to user-1 that is used to smooth the spectrum, $a_l^{(1)} \in \{\pm1\}$ is the user phase information and can only be detected by the coherent receivers, whereas $d_l^{(1)} \in \{0,1\}$ carries the user position information that can be seen by both coherent and noncoherent receivers, where $\delta_p = T_s/2$ is the position shift parameter.

$c_l^{(1)} \in \{0,1\}$ are the TH integers values that scramble the position of the burst for multiuser interference suppression. The condition

$$c_{max}T_b + T_d \leq \delta_p \qquad \textbf{(2.3)}$$

should be satisfied in order to prevent inter-symbol interference, where c_{max} is the maximum time hopping shift integer value and T_d is the maximum channel delay spread. Therefore, guard time T_g should set as follows

$$T_g \geq T_d + c_{max}T_b \qquad \textbf{(2.4)}$$

Accordingly, this combined modulation is regarded as BPSK/BPPM given in Figure 2.2, and depicted for $N_b = 5$, $T_s = 32T_b$, $\delta_p = 16T_b$, $T_g = 8T_b$ and $c_{max} = 7$ for two cases in order to illustrate the data transmit structure, TH effect and guard times. Here, $a_l = 1$ is assumed for both cases.

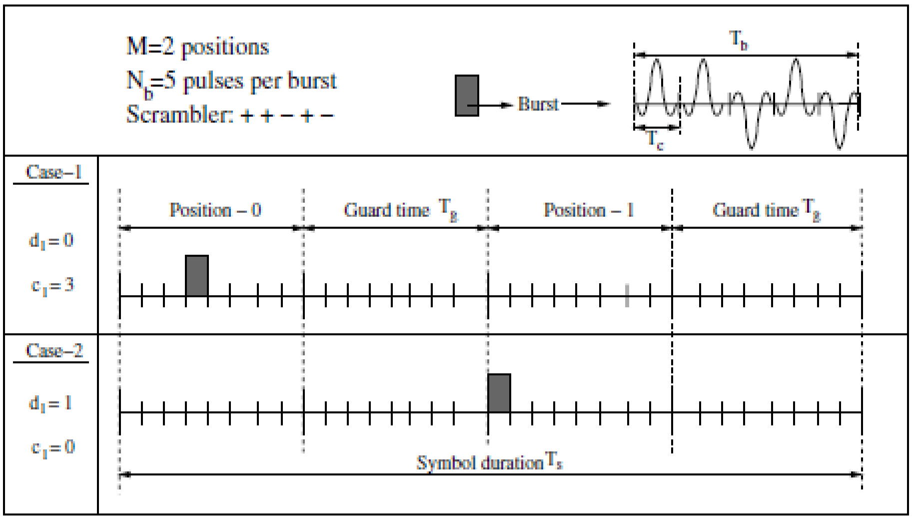

Figure 2.2 : Transmit structure of BPSK/BPPM [25].

In order to prevent inter-pulse interference and to specifically evaluate the effect of linear combination of pulses, it is assumed that a single user is active and a single pulse is transmitted. That means N_b is set to 1 without loss of generality. Thus, the transmitted signal can be simplified to

$$w_l^{(1)}(t) = a_l^{(1)} p\left(t - lT_s - d_l^{(1)}\delta_p\right) \qquad \textbf{(2.5)}$$

The received signal is subject to channel effects, primary user interference and the additive white Gaussian noise and can be modeled as

$$r(t) = \tilde{w}_l^{(1)}(t) + J(t) + n(t) \quad \textbf{(2.6)}$$

where $\tilde{w}_l^{(1)}(t)$ is the received waveform of the 1st user's l^{th} symbol, $J(t)$ represents the primary user signal, and $n(t)$ is the additive white Gaussian noise term with two-sided power spectral density $N_o/2$. The signal $\tilde{w}_l^{(1)}(t)$ is the waveform distorted by the channel $h(t)$ and is represented as

$$\tilde{w}_l^{(1)}(t) = \mathrm{w}_l^{(1)}(t) * h(t) \quad \textbf{(2.7)}$$

where * is the convolution operator. In the following, the interference model and the channel model that affect the received signal will be consecutively presented.

2.2 Interference Model

The licensed systems, indeed seen as interferences from the perspective of UWB systems will be modeled as single-tone or OFDM signals.

2.2.1 Single tone narrowband interference

TDMA, is a common media access that is used for various conventional wireless system such as GSM, IS-136, and in the DECT standard for portable phones.
Coexisting such licensed systems can be modeled as a single narrowband interference [22]

$$J(t) = \sqrt{2J_o}cos(2\pi f_j t + \theta_j) \quad \textbf{(2.8)}$$

where J_0 is the average power, f_j is the carrier frequency and θ_j is the random phase uniformly distributed over $[0,2\pi)$.

2.2.2 Wideband interference

OFDM is a common modulation scheme that is used for various wireless system LANs such as IEEE 802.11a. In addition, the OFDM based WiMAX system standardized in IEEE 802.16e is also expected to be a next generation mobile and wireless MAN system since it has advantages for the occupied bandwidth, data rate and anti-multipath effects, etc.

Coexisting OFDM based licensed systems can be modeled as a summation of multiple narrowband interferences [26]

$$J(t) = \sqrt{\frac{2J_o}{N}} \sum_{n=0}^{N-1} e^{j2\pi\left(n\Delta f + f_j\right)t + \theta_j} \qquad \textbf{(2.9)}$$

where N is the number of subcarriers in the OFDM signal and, Δf represents the subcarrier frequency spacing. The IEEE 802.16e standard uses scalable OFDMA to carry data, supporting channel bandwidths of between 1.25 MHz and 20 MHz, with up to 2048 sub-carriers [26].

The other major effect on the received signal is the channel effect and is presented next.

2.3 IEEE 802.15.4a Channel Model

Signal propagation in a wireless communication channel environment is made through multipath. Multipath fading channel distorts the received signal. In narrowband systems, multipath components cause self-interference, resulting in offset or reinforced reception. As to numerous multipath components, the amplitude of signal follows the Rayleigh distribution [27].

As the UWB systems have wide bandwidth, only several multipath components overlap with each other. Hence, it is not possible to apply the central limit theorem, which means that it is not possible to apply the Rayleigh distribution that is usually used for mobile telecommunication channel models [28]. The following has been suggested to model UWB channel: Cassioli divided the UWB channel into large-scale fading and small-scale fading, and presented a probability density function that coincided with the measured results. Large-scale fading includes the pathloss due to distance and shadowing. Cassioli [29] expressed the small-scale fading in Nakagami distribution, and Hashemi [30] used the log-normal distribution. In addition, Forest [31] proposed UWB channel model to IEEE, based on Saleh Valenzuela model, which was able to represent RMS delay, mean access delay, and the number of multipath components. This model represents the statistical chacteristics of the amplitude of multipath components and delay time [32].

Most of the work has been performed in the area of narrowband channel modeling and characterization, whereas channel modeling for UWB systems is relatively a new area. The narrowband channel models can not be generalized to UWB channels due to some important differences as described in [33]:

- Each multipath component can lead to delay dispersion by itself, due to frequency-selective nature of reflection and diffraction coefficients. This effect is especially important for systems with large relative bandwidth.
- The signals are received with excellent delay resolution. Therefore, it often happens that only a few multipath components make up one resolvable multipath component. That implies that the central limit theorem is not ful-filled anymore, and the amplitude statistics of such a resolvable multipath component is not complex Gaussian anymore. Similarly, there is an appreciable probability that areas of no energy can exist during which no significant amount of energy is arriving at the receiver.
- The statistics of arrival times of multipath components strongly vary with the bandwidth, as well as with the center frequency of considered signal.
- Due to wide frequency band, the propagation signal experiences frequency dependent effects. Specifically, the path loss described as a function of frequency as well as of distance when the relative bandwidth is large.

Considering the many measurements campaigns and the mathematical models, the IEEE 802.15.4a group has proposed a channel model for sensor networks and similar devices with data rates between 1 Kbps and several Mbit/s [34]. The important features of the channel model are presented in the Appendix.

Equivalent channel model *h(t)* can be given as

$$h(t) = \sum_{i=0}^{L-1} h_i \delta(t - \tau_i) \qquad \textbf{(2.10)}$$

where h_i is the i^{th} multipath channel coefficient, τ_i is the delay of the i^{th} multipath component and $\delta(.)$ is the dirac delta fuction. Consistent with earlier studies, it is assumed that the channel coefficients are normalized

$$\sum_{i=0}^{L-1} \mathrm{h}_i^2 = 1 \qquad \textbf{(2.11)}$$

to remove the path loss effect, and that the delays $\{\tau_i\}$ occur at the integer multiples of the chip time T_c.

The IEEE 802.15.4a channel models cover different measured indoor residential, indoor office, industrial, outdoor, and open outdoor environments. Among the channel models, *CM1* (indoor residential line-of-sight (LOS)), *CM5* (outdoor LOS) and *CM8* (industrial non-LOS (NLOS)) channel models, are widely used in UWB research. The characteristics of channel models *CM1*, *CM5* and *CM8* are summarized in the following.

***CM1*: This is by far the most commonly used channel model in order to assess the system performance. It models an LOS connection in an indoor residential environment. These environments are critical for home networking, linking different appliances, as well as safety fire, smoke sensors over a relatively small area. The building structures of residential environments are characterized by small units, with indoors walls of reasonable thickness.

***CM5*:** This is a channel model with an LOS connection in an outdoor environment. While a large number of different outdoor scenarios exist, the current model covers only a suburban-like microcell scenario, with a rather small range.

***CM8*:** This is a channel model with an NLOS connection in an industrial environment characterized by larger enclosures factory halls, filled with a large number of metallic reflectors. This is anticipated to lead to severe multipath.

Typical channel realization of each channel model is plotted in Figure 2.3.

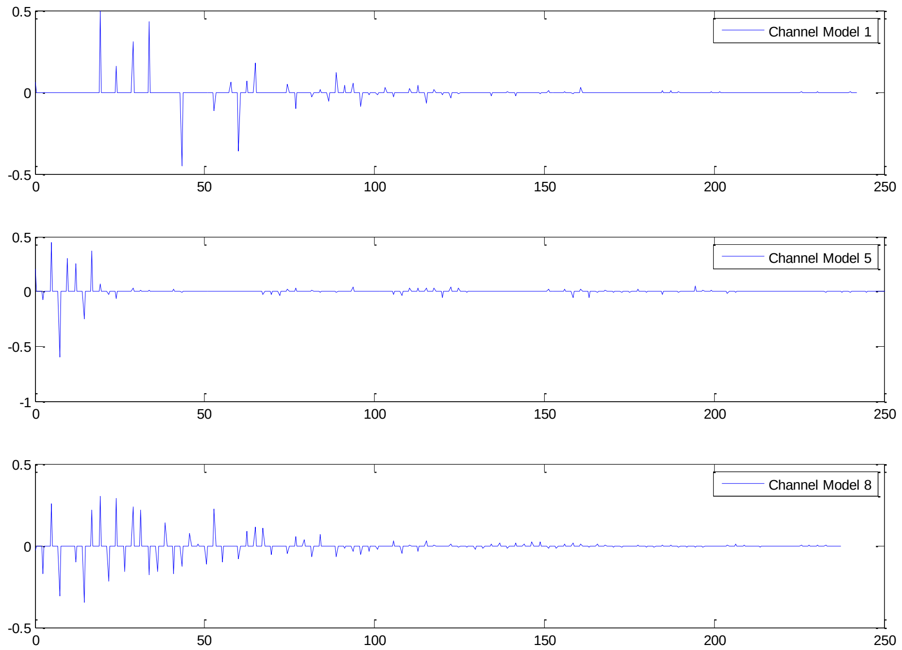

Figure 2.3 : Typical channel realizations for *CM1*, *CM5* and *CM8*.

Also, in the literature, channel model effects on the system performance are studied [35]. Energy collection performance of *CM1*, *CM5* and *CM8* is given in Figure 2.4. *CM1* has short-lasting channel delay spread and a few channel coefficients. Owing to these features, *CM1* collects the channel energy fastest. On the other hand, it is observed that in the realizations of *CM5*, multipath components arrive in two or more separate clusters. As a result, as shown in Figure 2.4, initially *CM5* energy collection rate is greater than *CM8*. However, after about 25 ns the energy collection rates are reversed.

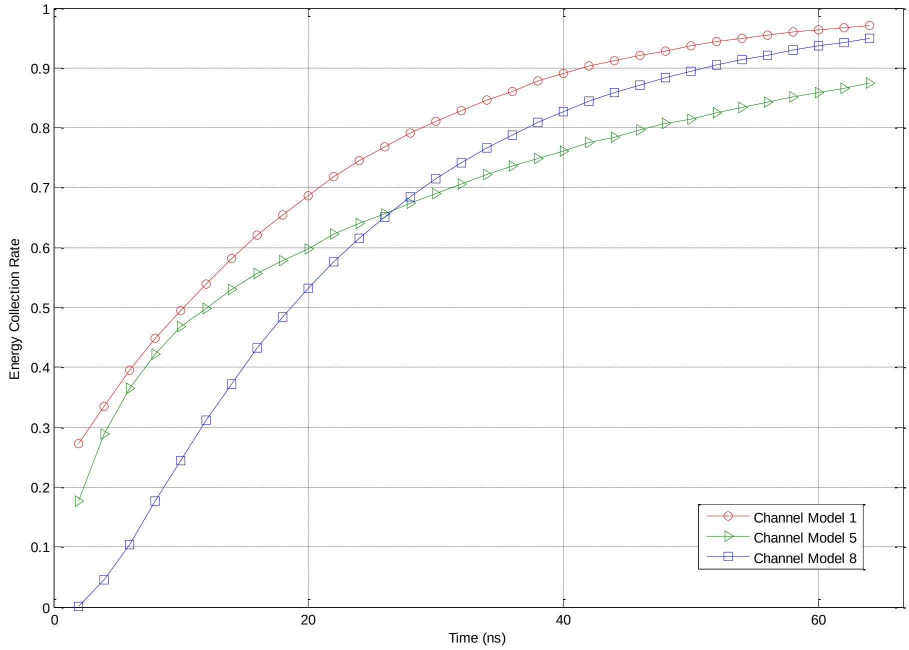

Figure 2.4 : Energy collecting performance in *CM1*, *CM5* and *CM8*.

2.4 Conventional Receiver Structures

The amount of multipath energy that can be collected at the receiver, and the receiver complexity are commonly used to determine the performance and robustness of a wireless communication system. At the receiver, the information of user-1 transmitted by binary phase shift keying and binary pulse position modulation can be detected either coherently or noncoherently. In the following, how the received signal in **(2.6)** can be processed with two receiver structures, are presented.

2.4.1 Coherent receiver

The coherent receiver is a Rake receiver used in any kind of spread spectrum communication system to accumulate the energy in the significant multipath components. The use of Rake receivers in UWB systems is also common to collect the available rich multipath diversity.

A Rake receiver implemented using the delayed versions of the reference signal is shown in Figure 2.5.

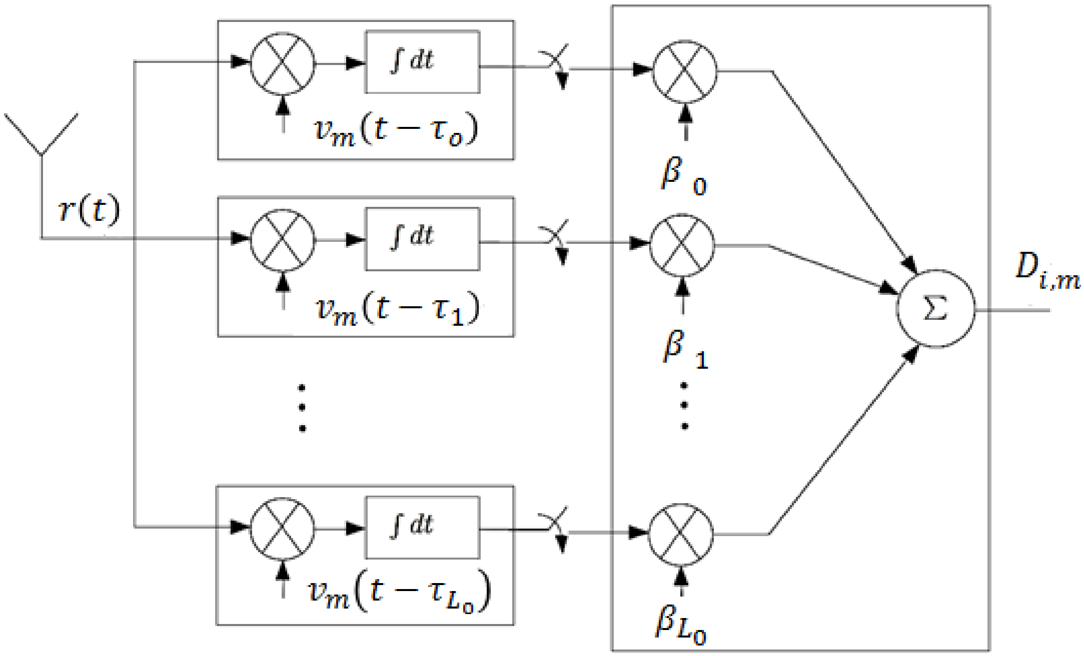

Figure 2.5 : A Rake receiver structure for TH-IR UWB system [36].

It consists of a bank of correlators, also called fingers, and each finger is matched and synchronized to a particular multipath component to combine the received multipaths coherently. In order to enable symbol-rate sampling, the received UWB-IR signal which is specified in **(2.6)** can be correlated with a symbol-length template signal, and the correlator output can be sampled once per symbol [37]. The output of the correlator corresponding to the i^{th} finger of Rake receiver for the m^{th} pulse position can be given by

$$D_{i,m}^{(1)} = \int_{-\infty}^{\infty} r(t) v_m\,(t-\tau_i)dt$$

$$= \int_{-\infty}^{\infty} \left(\widetilde{w}_l^{(1)}(t) + J(t) + n(t)\right) v_m\,(t-\tau_i)dt \quad \textbf{(2.12)}$$

i=0 ,…, L_0-*1* for *m*=0,1, where

$$v_m(t) = p(t - lT_s - m\delta_p) \tag{2.13}$$

is the reference signal and L_0 is the number of Rake fingers used.

The drawback of Rake receiver is that the number of multipath components that can be utilized in a typical Rake combiner is limited by power consumption issues and the design complexity. Also the channel in UWB systems causes distortion in the received pulse shape and makes the use of a single LOS path signal as a suboptimal template [38].

A tapped delay line channel with *K* number of delays provides with *K* replicas of the same transmitted signal at the receiver. Hence, a receiver that processes the received signal in an optimum manner will achieve the performance of an equivalent K^{th} order diversity system. In practice, only a subset of total resolved multipath components is used in the Rake receivers [39].

Hence, the Rake receiver processing can be classified as follows:

All Rake : The Rake receiver which combines all the *K* resolved multipath components is called an all Rake (A-Rake) receiver.

Selective Rake : The selective Rake (S-Rake) receiever searches for the L_0 best paths out of *K* resolved multipath components to use them in Rake fingers.

Partial Rake : The partial Rake (P-Rake) receiver uses the first arriving L_0 paths out of *K* resolvable multipath components.

In this thesis, P-Rake is used due to receiver simplicity.

The outputs of the correlators or fingers are passed to the Rake combiner. The Rake receiver can use different combining schemes such as maximal ratio combining and equal gain combining.

If maximal ratio combining technique is used, the amplitudes of the received multipath components are estimated and used as weighting vector in each finger.

The performance and optimality of the maximal ratio combining consequently depend upon the receiver's knowledge of the channel [38]. Let $\boldsymbol{\beta} = [\beta_0, \beta_{1,\dots,} \beta_{K-1}]$ be the Rake combining weights which are different for different Rake types.

In case of P-Rake, using the first L_0 multipath components, the weights of maximal ratio combining are given by

$$\beta_i = \begin{cases} h_i, & i = 0, \dots, L_0 - 1 \\ 0, & i = L_0, \dots, K - 1 \end{cases} \qquad \textbf{(2.14)}$$

where $L_0 \leq K$.

In case of equal gain combining scheme, all tracked multipath components are weighted with their corresponding signs and combined. Thus equal gain combining scheme only requires the phase of the fading channel [40]. In a carrierless UWB system, determining the phase is even simpler because the phase is either 0 or π, to account for pulse inversion [41]. In a practical system, performing equal gain combining will be simpler than maximal ratio combing however, there will be a performance trade-off.

Assuming that the channel parameters can be predicted, a maximal-ratio combiner is used to combine the Rake receiver outputs as

$$D_m^{(1)} = \sum_{i=0}^{L_0-1} h_i \, D_{i,m}^{(1)} \qquad \textbf{(2.15)}$$

to form the decision variables. Since $\{D_m^{(1)}\}$ carries the phase information as well, the data is recovered as

$$\max\{|D_m^{(1)}|\} = D_{d_l'}^{(1)} \Rightarrow d_l' \qquad \textbf{(2.16)}$$

$$sign\left\{D_{d_l'}^{(1)}\right\} \Rightarrow a_l' \qquad \textbf{(2.17)}$$

where $|x|$ and sign $\{x\}$ denote the absolute value and the sign of x, respectively.

2.4.2 Noncoherent receiver

The noncoherent receiver is an energy detector with the decision variables $\{D_m^{(1)}\}$ where

$$D_m^{(1)} = \int_{m\delta_p}^{m\delta_p+T_i} r^2(\mathrm{t})\, dt$$

$$= \int_{m\delta_p}^{m\delta_p+T_i} \left(\widetilde{w}_l^{(1)}(t) + J(t) + n(t)\right)^2 dt \qquad \textbf{(2.18)}$$

with m = 0,1, which integrates the received signal energy for the duration of T_i. The position information is recovered by finding the maximum decision variable as

$$\max\{|D_m^{(1)}|\} = D_{d_l'}^{(1)} \Longrightarrow d_l' \qquad \textbf{(2.19)}$$

Here, the performance will mainly depend on the noise and interference levels, as well as the appropriate integration times T_i. There have been studies which try to find the optimum integration times [42].

Compared to the coherent receiver, this is a very simple receiver structure. On the other hand, this brings the following disadvantages:

- Only 1-bit can be recovered. Phase information cannot be obtained.
- Signal-noise cross-terms and noise squared terms deteriorate the detection performance.

3. MODIFIED TRANSCEIVER STRUCTURE

In case of an active primary system sharing the same frequency band, the UWB system has to take an action. The UWB can either use detect-and-avoid techniques, or use pulses that have lower spectra at the primary systems' frequency bands. If the primary system is active most of the time, using detect-and-avoid techniques may decrease the operation time of UWB systems significantly. Accordingly, the IEEE 802.15.4a standard suggests using linear combination of pulses. Hence, implementation of the linear combination of pulses are considered to reduce the power level at the desired frequency of a narrowband system, front-end filter matched to the linearly combined pulse at the receiver is considered before coherent or noncoherent receiver processing.

In this chapter, the modified transceiver structure resulting from above structure is presented. First, the implementation method of the linear combination of pulses is introduced in Section 3.1. Then, possible linearly combined pulses that conform to the IEEE 802.15.4a standard is presented in Section 3.2. Finally, receiver processing is presented for both coherent and noncoherent modifed receiver in Section 3.3.

3.1 Linear Combination of Pulses

The linear combination of pulses as defined in the IEEE 802.15.4a standard is

$$p_{lcp}(t) = \sum_{n=0}^{N-1} a_n p(t - \tau_n) \quad \textbf{(3.1)}$$

where $p(t)$ is a standard pulse used in the data transmission, $a_n \in$ [-1,1] are the pulse coefficients, τ_n is pulse delay, N is the number of pulses to be used and $p_{lcp}(t)$ is the the new pulse shape formed by linear combination of standard pulse.

According to the standard, the maximum number of pulses is limited by 4, and pulse delays are restricted to $0 \leq \tau_n \leq$ 4ns with τ_0 = 0. The new pulse shape given in **(3.1)** has the frequency domain representation

$$P_{lcp}(f) = \sum_{n=0}^{N-1} a_n e^{-j2\pi f \tau_n} P(f)$$

$$= P(f).C(f) \qquad \textbf{(3.2)}$$

where $P(f)$ is the pulse spectrum and $C(f)$ is the code spectrum which is independent from the pulse spectrum.

As mentioned before, pulse design techniques for utilizing spectral mask efficiently have been extensively studied in the literature. In this thesis, independent from pulse design only the effect of code spectrum is investigated.

In code spectrum design, widely preferred FIR filters are used . Therefore, delays of the consecutive pulses are equidistant. This design can be achieved by using different methods (e.g., Parks- McClellan method, windowing method, etc.) [43]. However, mentioned methods require a large number of coefficients. Since the main approach is code spectrum design with the least number of filter coefficients which is equivalent to limited number of linearly combined pulse for complying IEEE 802.15.4a standard, code spectrum can be obtained by placing one or more zeros on a z-transform unit circle [19].

Then code spectrum is defined as follows

$$C(f) = \sum_{n=0}^{N-1} a_n e^{-j2\pi f \tau_n}. \qquad \textbf{(3.3)}$$

By letting

$$z = re^{j2\pi f \tau_n}, \ (\mathrm{r} \ = 1) \qquad \textbf{(3.4)}$$

And using pulse delays periodic inversely proportional to the sampling frequency,

$$\tau_n = \frac{n}{f_s} \qquad \textbf{(3.5)}$$

the z-transform of the code spectrum becomes

$$C(z) = \sum_{n=0}^{N-1} a_n z^{-n} \qquad \textbf{(3.6)}$$

The usage of z-transform for obtaining desired notch at f_1 frequency is illustrated in Figure 3.1.

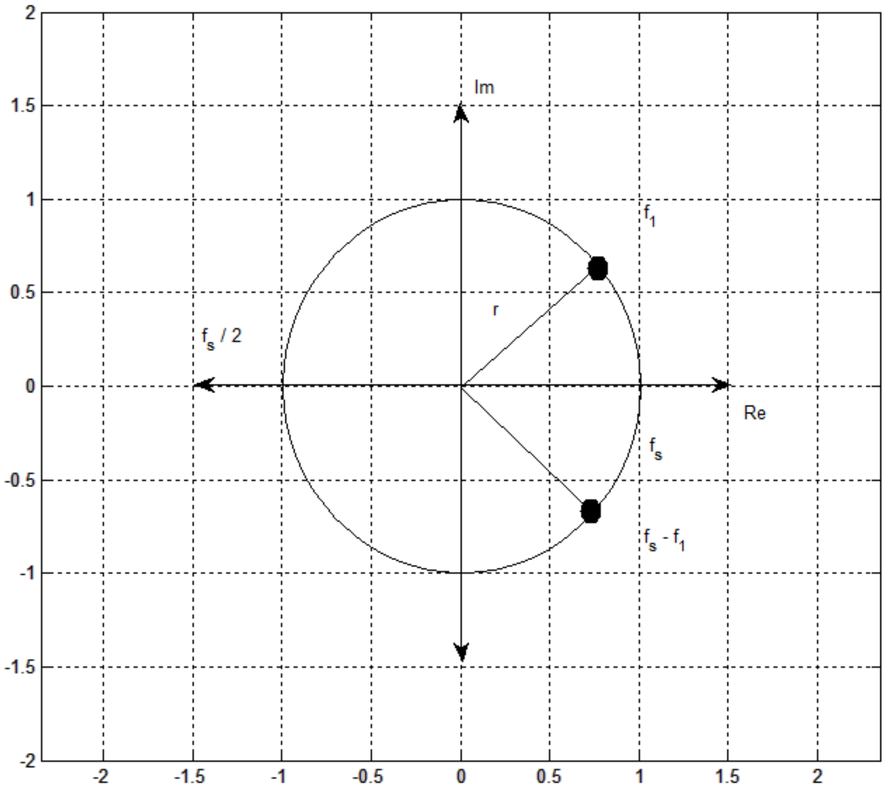

Figure 3.1 : Illustration of obtaining notches at desired frequency $f_{1.}$

Accordingly, when a zero is placed at f_1 frequency on a unit circle, another zero shall also be placed at the complex conjugate of f_1 for obtaining real filter coefficients. As shown in the Figure 3.1, it turns out another notch at f_s-f_1

$$C(z) = \left(\mathrm{z} - \mathrm{r}e^{j2\pi\left(\frac{f_1}{f_s}\right)}\right)\left(\mathrm{z} - \mathrm{r}e^{-j2\pi\left(\frac{f_1}{f_s}\right)}\right)$$

$$= z^2 - 2rcos\left(2\pi\left(\frac{f_1}{f_s}\right)\right)z + r^2$$

$$= 1 - 2rcos\left(2\pi\left(\frac{f_1}{f_s}\right)\right)z^{-1} + r^2z^{-2}. \quad \textbf{(3.7)}$$

Since the zeros are on the unit circle (i.e., r=1), the code spectrum coefficients are a_0= 1, $a_1 = -2cos\left(2\pi\left(\frac{f_1}{f_s}\right)\right)$ and a_2 = 1.

In the following, code spectrum design of various linear combination of pulses are investigated.

3.2 Possible Linearly Combined Pulses

As the IEEE 802.15.4a standard limits the number of pulses to N = 4, only a single primary user can be avoided. As a result, four different types of possible combined pulses are considered.

3.2.1 Linearly combined pulse-0

Initially, placement of a single zero at sampling frequency f_s on the z-plane is considered which is given Figure 3.2.

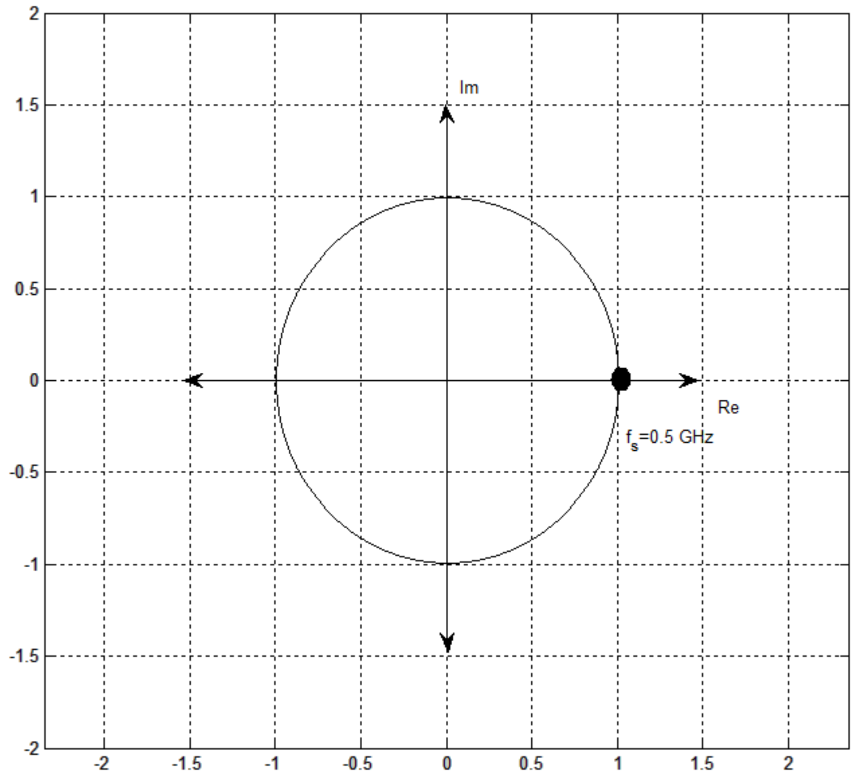

Figure 3.2 : N=2, single zero placed at f_s = 500 MHz.

With the least number of pulse coefficients (two) $\{a_n\}$, a notch at the frequency $f_n = f_s$ and also integer multiples of f_s can be obtained by selecting pulse coefficients a_0 = 1, a_1 = -1 and $\tau_1 = \frac{1}{f_s}$ respectively. The new pulse becomes

$$p_{lcp0}(t) = p(t) - p\left(t - \frac{1}{f_s}\right) \quad \textbf{(3.8)}$$

In Figure 3.3, magnitude spectra of the standard pulse given in **(2.1)** and the linearly combined pulse given in **(3.8)**, i.e., $P(f)$ and $P_{lcp}(f)$ are plotted when f_s= 500 MHz. The notch frequencies can be obtained at multiples of 500 MHz.

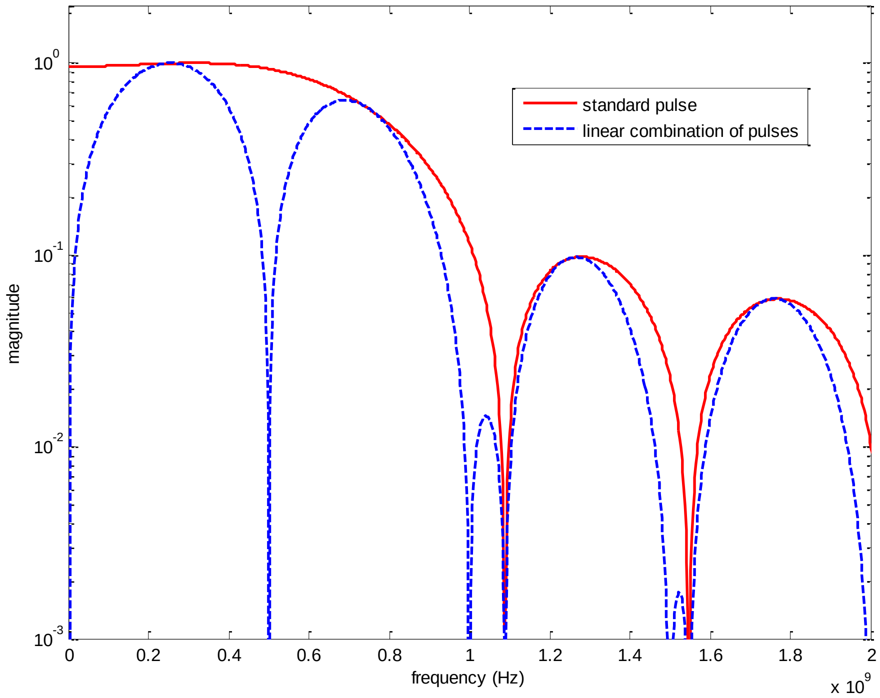

Figure 3.3 : Magnitude spectra of the standard and the linearly combined pulses.

3.2.2 Linearly combined pulse-1

Secondly, placement of a single zero at sampling frequency $f_s/2$ on the z-plane is considered which is given Figure 3.4.

With the least number of pulse coefficients $\{a_n\}$, a notch at the frequency $f_n = f_s/2$ and also odd integer multiples of f_n can be obtained by selecting pulse coefficients $a_0 = a_1 = 1$ and $\tau_1 = \frac{1}{f_s}$. The new pulse becomes

$$p_{lcp1}(t) = p(t) + p\left(t - \frac{1}{f_s}\right) \quad \textbf{(3.9)}$$

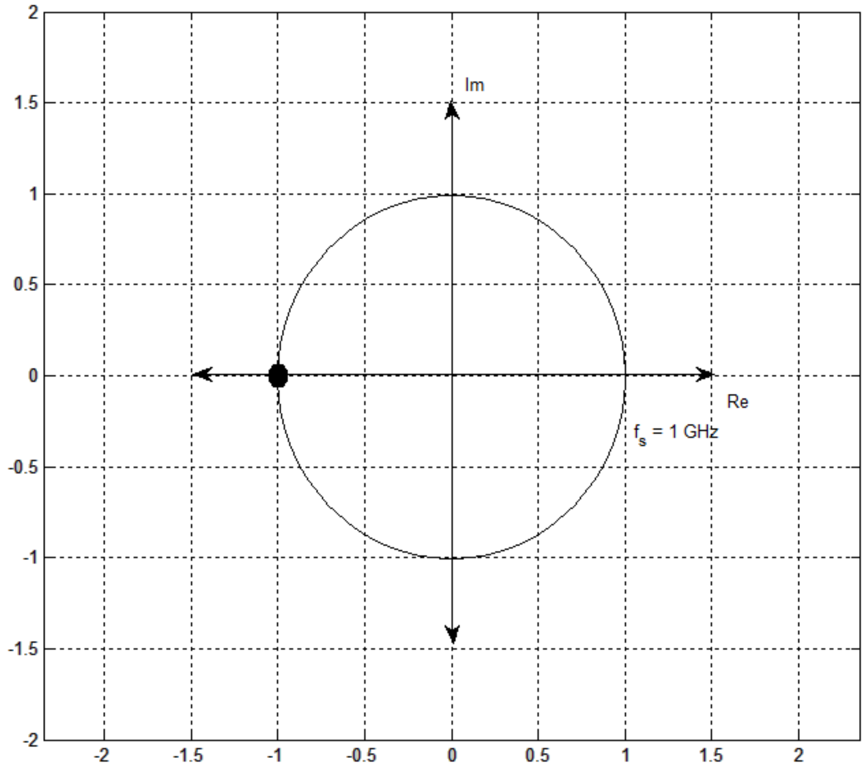

Figure 3.4 : N=2, single zero placed at $f_s/2$= 500 MHz.

3.2.3 Linearly combined pulse-2

Thirdly, placement of double zeros at sampling frequency $f_s/2$ on the z-plane is considered which is given Figure 3.5. This pulse is expected to have wider notch at the center frequency of a primary system.

With the least number of pulse coefficients $\{a_n\}$, a notch at the frequency $f_n = f_s/2$ and also odd integer multiples of f_n can be obtained by selecting pulse coefficients a_0= 1, a_1= 2 and a_2= 1, $\tau_1 = \frac{1}{f_s}$ and $\tau_2 = \frac{2}{f_s}$. The new pulse becomes

$$p_{lcp2}(t) = p(t) + 2p\left(t - \frac{1}{f_s}\right) + p\left(t - \frac{2}{f_s}\right) \qquad \textbf{(3.10)}$$

In Figure 3.6, a portion of the spectra is plotted for $p_{lcp1}(t)$ and $p_{lcp2}(t)$. It can be observed that the $p_{lcp2}(t)$ may accommodate the wideband systems better with its wider notch at f_n = 500 MHz.

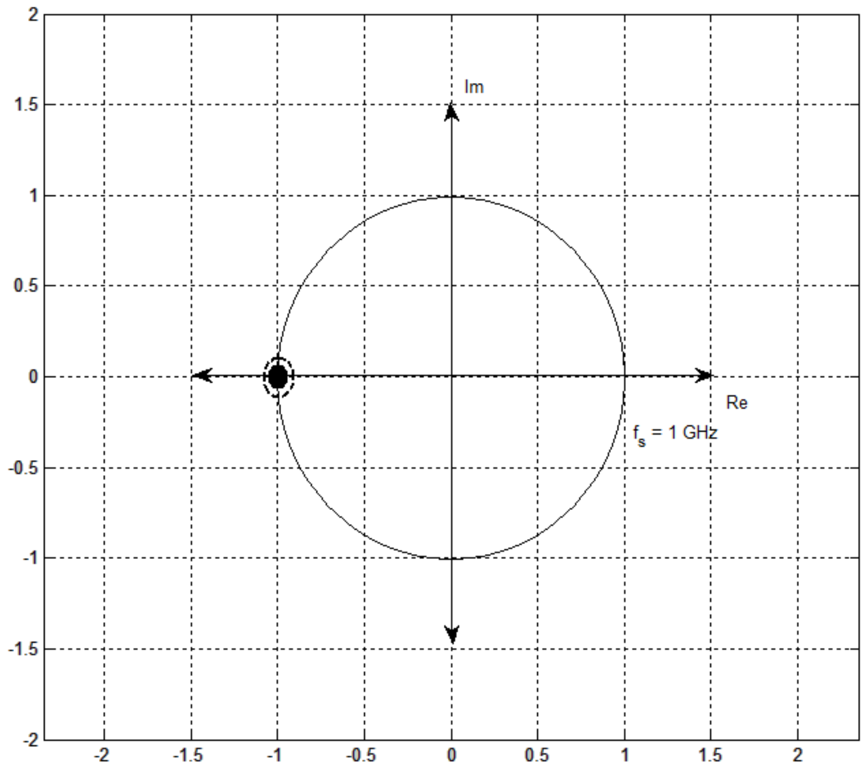

Figure 3.5 : $N=3$, double zeros placed at $f_s/2$= 500 MHz.

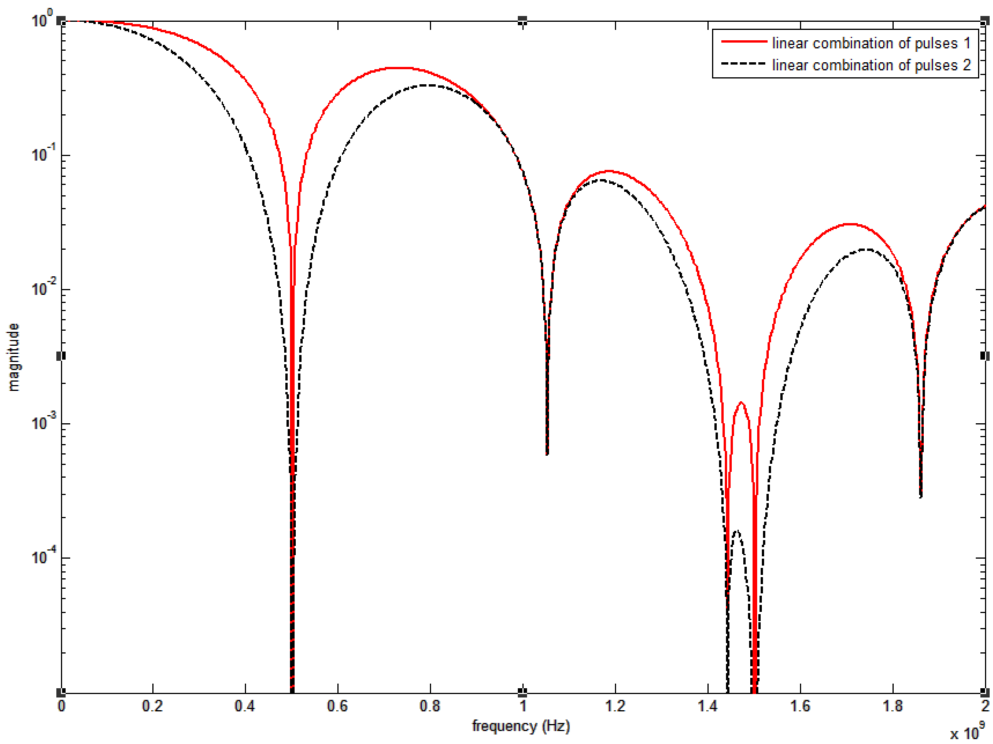

Figure 3.6 : Magnitude spectra of the lcp_1 and the lcp_2.

3.2.4 Linearly combined pulse-3

Finally, placement of triple zeros at $f_s/2$ on the z-plane is considered which is given Figure 3.7.

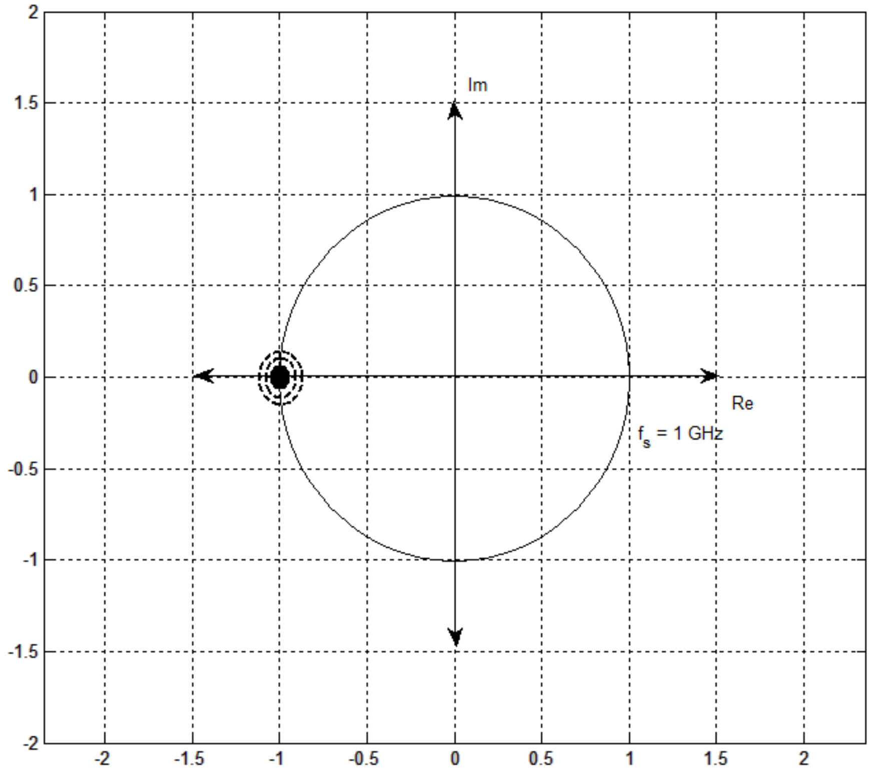

Figure 3.7 : N=4, triple zeros placed at $f_s/2$= 500 MHz.

With four pulse coefficients, which is the upper limit allowed to be used, the widest notch at the frequency f_n and also odd integer multiples of $f_n = f_s/2$ can be obtained by selecting pulse coefficients a_0= 1, a_1= 3 and a_2= 3 and a_3= 1, $\tau_1 = \frac{1}{f_s}$, $\tau_2 = \frac{2}{f_s}$ and $\tau_3 = \frac{3}{f_s}$, resulting in

$$p_{lcp3}(t) = p(t) + 3p\left(t - \frac{1}{f_s}\right) + 3p\left(t - \frac{2}{f_s}\right) + p\left(t - \frac{3}{f_s}\right). \qquad \textbf{(3.11)}$$

3.3 Modified Receiver Structures

Since the UWB system shares the spectrum with a primary user $J(t)$, it first has to modify its pulse shape to $p_{lcp}(t)$ in order to minimize the interference to primary system.

Then at the receiver, the received signal should be matched to the transmitted pulse shape before it can be further processed with a coherent or a noncoherent detector. The modified transceiver structure is shown in Figure 3.8

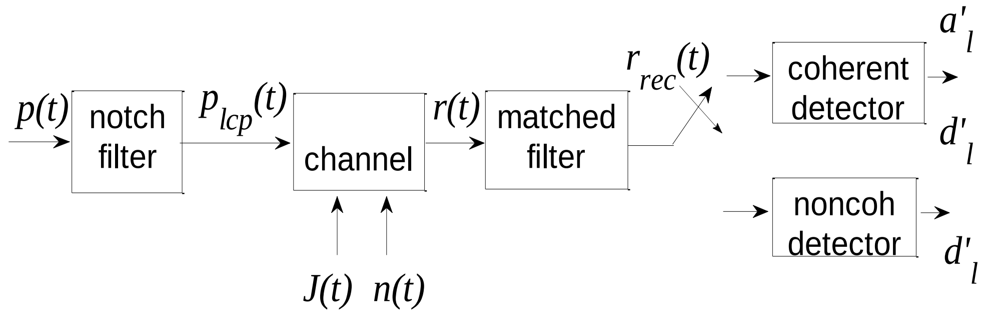

Figure 3.8 : Block diagram of the modified transceiver structure.

3.3.1 Coherent receiver

For the coherent receiver structure, the signal at the output of the matched filter is

$$r_{rec}(t) = r(t) * p_{lcp}(-t) \quad \textbf{(3.12)}$$

The useful signal component of $r_{rec}(t)$, can be obtained from $\tilde{w}_l^{(1)}(t) * p_{lcp}(-t)$, where $\tilde{w}_l^{(1)}(t)$ consists of time shifted pulses $p_{lcp}(t)$. Therefore, the correlation-based coherent receiver should use

$$v_{mrec}(t) = v_m(t) * p_{lcp}(-t) \quad \textbf{(3.13)}$$

as the new reference signal to obtain the correlator outputs as

$$D_{i,m}^{(1)} = \int_{-\infty}^{\infty} r_{rec}(t) v_{mrec}(t - \tau_i) dt$$

$$= \int_{-\infty}^{\infty} \Big((\tilde{w}_l^{(1)}(t) + J(t) + n(t)) * p_{lcp}(-t) \Big) \Big((\tilde{w}_l^{(1)}(t) + J(t) + n(t)) * p_{lcp}(-t) \Big) dt \quad \textbf{(3.14)}$$

Then **(2.16)** and **(2.17)** can be used to detect the transmitted bits.

3.3.2 Noncoherent receiver

For the noncoherent receiver structure, energy detectors can be used and only the BPPM bit can be recovered. In the presence of interference, the noncoherent receiver structure needs to filter the interference at the front-end before performing energy detection.

Accordingly, the matched filtered signal $r_{rec}(t)$ given in **(3.12)** can be directly used in

$$D_m^{(1)} = \int_{m\delta_p}^{m\delta_p+T_i} (r_{rec}(\mathrm{t}))^2 \, dt$$

$$= \int_{m\delta_p}^{m\delta_p+T_i} \left((\widetilde{w}_l^{(1)}(t) + \mathrm{J(t)} + \mathrm{n(t)}) * p_{lcp}(-t) \right)^2 dt \quad \textbf{(3.15)}$$

for the noncoherent receiver. The bit then can be detected using **(2.19)**.

In the following, the performance of the IEEE 802.15.4a system will be evaluated for various pulse types, receiver structures and interference types.

4. RESULTS

In this chapter, the system performances are evaluated in terms of the bit error rate (BER) with respect to varying SNR and SIR values. The SNR and SIR are defined as E_b/N_o and E_b/J_o respectively, where E_b is the bit energy. It is assumed that the standard pulse used is a root raised cosine pulse with roll-off factor β = 0.6 and T_p= 2 ns duration as given in [14]. The linearly combined pulses are obtained from **(3.8)-(3.11)** and generate a notch at f_j= 500 Mhz, where there is either an active primary narrowband system given in **(2.8)** or an active wideband system as given in **(2.9)**. The *CM1*, *CM5* and *CM8* used are the standardized IEEE 802.15.4a channel models [34] with a channel resolution of T_c = 2 ns.

The UWB system performance is evaluated for both the coherent and non-coherent operation modes. As a benchmark, performances of the original (i.e., standard) pulse and the designed pulses are determined when there is no interference. The performances of both the original and designed pulses are studied in the presence of interference. The factors that affect the system performance can be listed as follows, and are tested under different scenarios.

i) IEEE 802.15.4a receiver structure (coherent and non-coherent)

ii) Pulse characteristics (pulse design coefficients)

iii) Interference types (narrowband, wideband and bandwidth/subcarriers)

4.1 Effects of transmitter-receiver structure

In this section, effects of the transceiver structure on the UWB system performance are presented for both coherent and noncoherent reception in the presence of a narrowband interference.

4.1.1 Coherent transmitter-receiver structure

Initially, the coherent receiver performance is assessed. In Figure 4.1, the BER performances are plotted for various SIR values when SNR = 15dB and 5-tap P-Rake receivers are used.

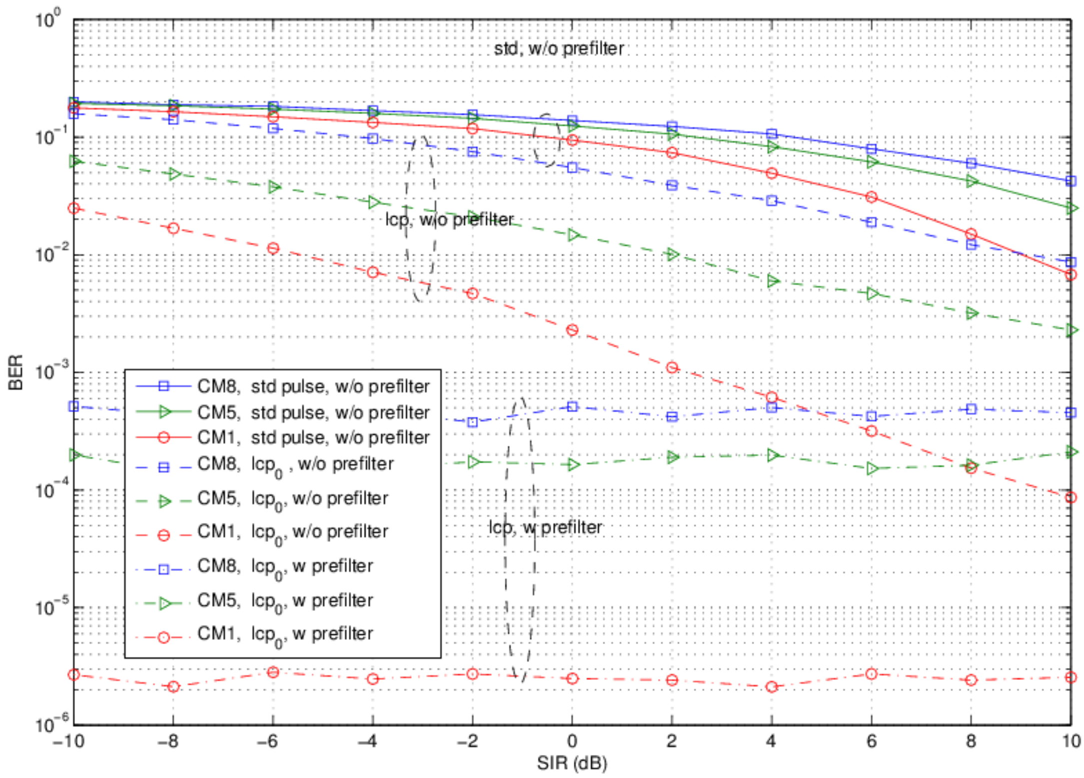

Figure 4.1: BER performance of 5-tap P-Rake receiver for various SIR values and transceiver when SNR=15 dB.

When a standard pulse is used and there is no prefiltering which means no matched filtering at the receiver front-end, the BER performance of the UWB system is poor for all SIR values and channel models. Note that this case is also unacceptable from the primary system's perspective due to high UWB interference level. When the linearly combined pulse-0 (lcp_0) is used instead of the standard pulse, the corresponding correlator template at the receiever provides an inherent rejection capability although it is limited. When prefilter is used as well, the narrowband interference is suppressed at all SIR values. It should also be noted that the performances are better in the order of *CM1*, *CM5* and *CM8* as expected.

In Figure 4.2, the BER performances are plotted for various SNR values when 5-tap P-Rake receivers are used.

When a standard pulse is used, the performances are the best when there is no active primary system. However if a narrowband system becomes active, the BER performance degrades drastically for both *CM1* and *CM8*. When lcp_0 is used, the performances are slightly worse than the standard pulse case when there is no interference.

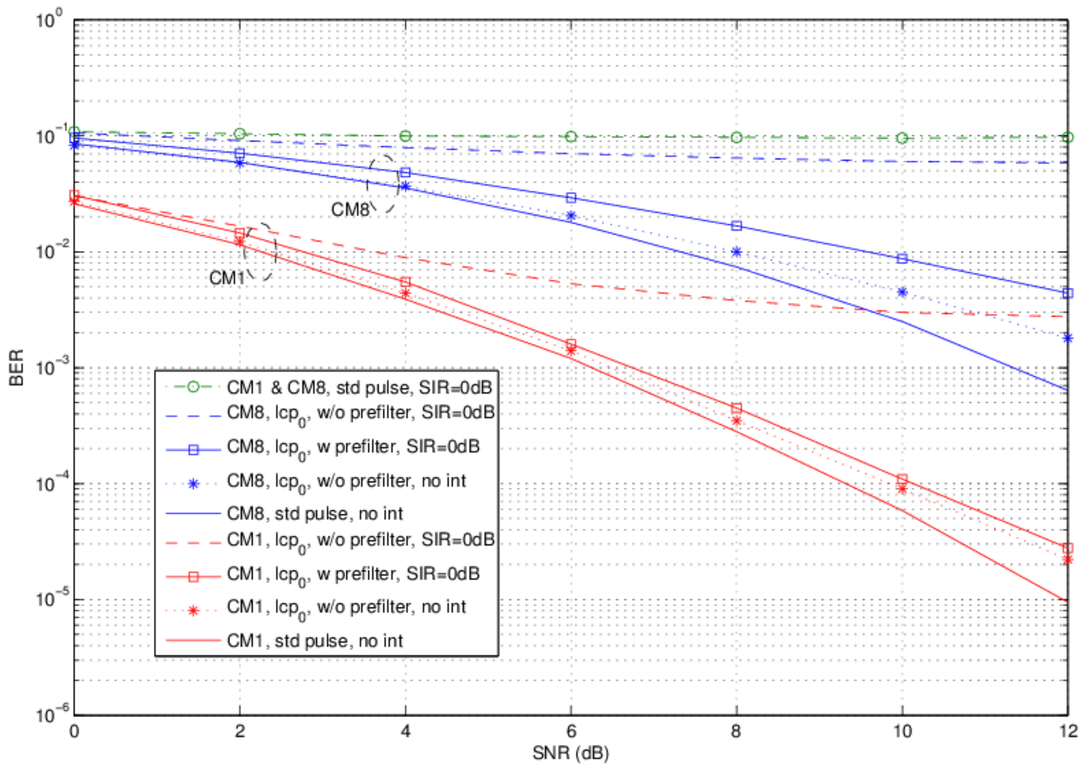

Figure 4.2 : BER performance of a 5-tap P-Rake receiver for various SNR values and transceiver structures.

This can be explained by the duration of the linearly combined pulse becoming longer than T_p = 2 ns, which is also the assumed channel resolution. Hence, the performance degredation is due to the inter-pulse interference caused by channel. When a narrowband system becomes active, while the linearly combined pulse with no prefiltering can provide some degree of interference suppression, including a front-end prefilter improves the performance close to the no interference case for *CM1* and *CM8*.

4.1.2 Noncoherent transmitter receiver structure

Next, the noncoherent receiver performance is assessed in *CM1* for lcp_0 and in the presence of a single-tone interference. In Figure 4.3, the BER performances are plotted for various SIR values when SNR=30 dB and noncoherent receivers are used.

When a standard pulse is used and there is no prefiltering, the BER performance of the UWB system is poor for all SIR values and integration durations.

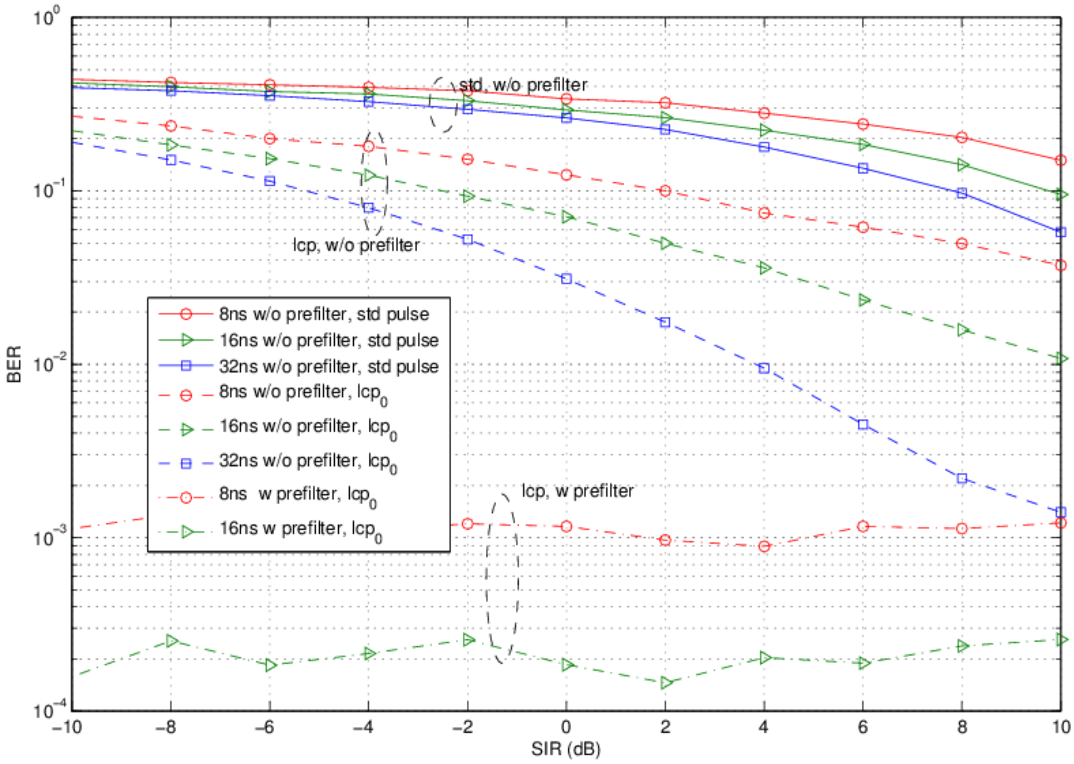

Figure 4.3 : BER performance of a noncoherent receiver in *CM1* for various and transceiver structures when SNR=30dB.

Similar to the coherent receiver case, using a linearly combined pulse improves the BER performance noticeably, whereas using also a prefilter at the front-end can suppress the interference independent from the SIR values.

In Figure 4.4, the BER performances are plotted for various SNR values when noncoherent receivers with different integration durations are used.

Here, the performance of a standard pulse when there is no interference serves as a benchmark. When a linearly combined pulse is used for the same conditions, the performances are worse about 0.5-1 dB compared to standard pulse. This is also due to the linearly combined pulse having a longer duration than the assumed channel resolution. If a narrowband system becomes active, the transceiver structure that uses the linearly combined pulse can activate the front-end prefilter and obtain 1-2 dB worse performance compared to standard pulse with no interference. It should also be noted that the performance improves with increased integration durations at high SNR values.

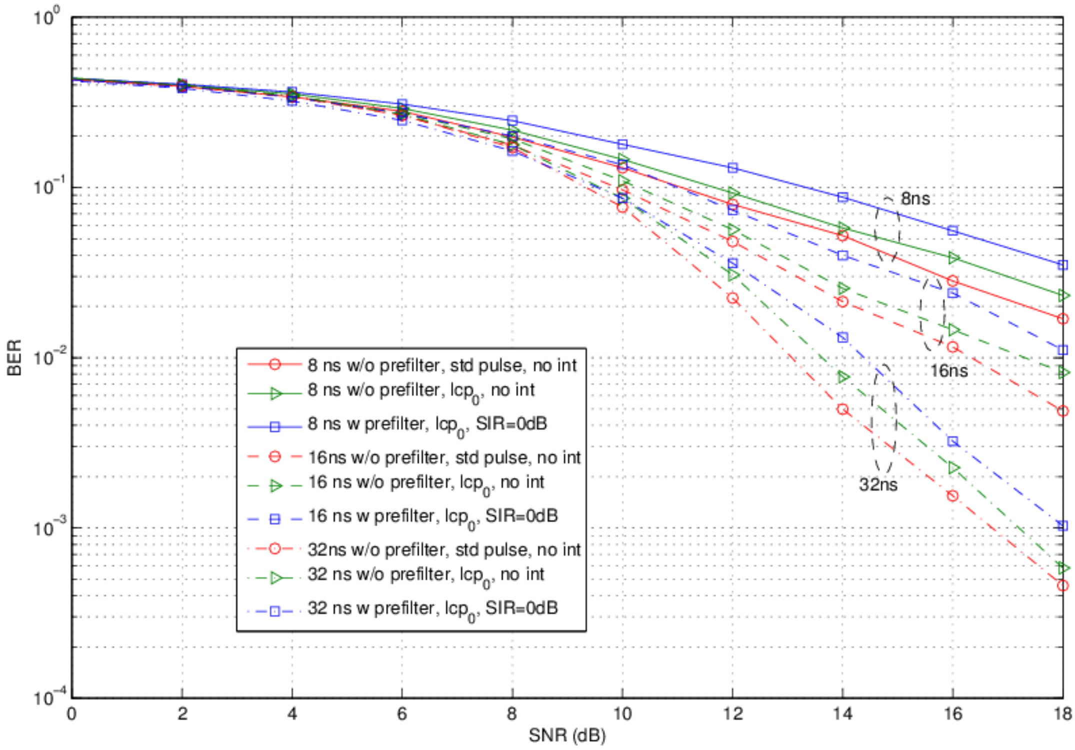

Figure 4.4 : BER performance of a noncoherent receiver in *CM1* for various SNR values and transceiver structures.

4.2 Effects of pulse types

In this section, effects of various linearly combined pulse types on the UWB system performance are presented for both coherent and noncoherent reception in the presence of wideband interference.

4.2.1 Coherent Receiver

The coherent receiver performances of linearly combined pulses lcp_0, lcp_1, lcp_2 and lcp_3 are assessed in the presence of a wideband interference with a bandwidth of 20 MHz and 16 subscarriers. In Figure 4.5, the BER performances are plotted for various SIR values when SNR = 15dB and 5-tap P-Rake receivers are used.

The performance of lcp_1 when there is no interference serves as a benchmark. When there is an active primary system, the performances of lcp_1, lcp_2, lcp_3 employing matched filters are similiar and slightly worse than ideal case. On the other hand, lcp_0 with prefilter performs poorly at lower SIR values because of it is narrower notch width.

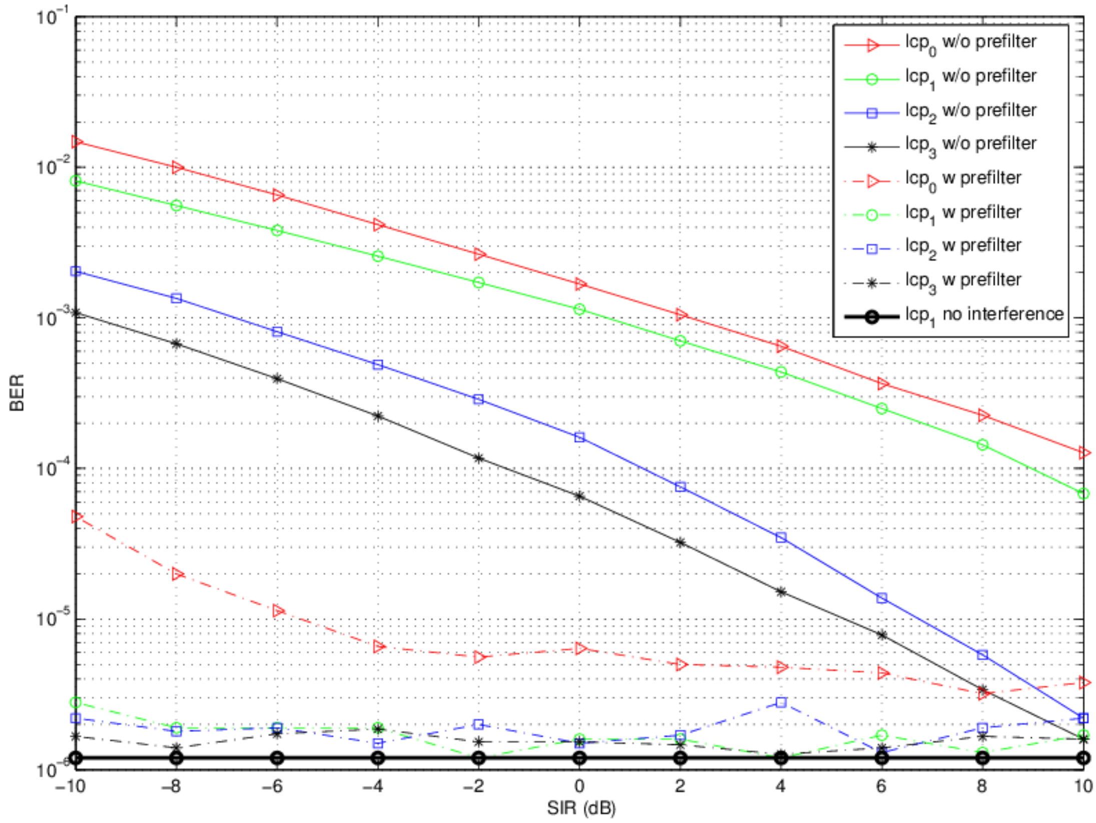

Figure 4.5 : BER performance of a coherent receiver in *CM1* for various SIR values and pulse types.

In addition, without prefiltering the performances improve in order of lcp_0, lcp_1, lcp_2, lcp_3. This can be explained by more effective spectrum utilization and accommodation of a wider notch.

In Figure 4.6, the BER performances are plotted for various SNR values when SIR = 0 dB and 5-tap P-Rake receivers are used for the same wideband interference.

The performance of lcp_3 when there is no interference serves as a benchmark. While sharing the same band with an active primary system, lcp_3 used with front end filtering shows 0.5-1 dB worse performance compared to the no interference case. This is also due to prefiltering structure not being able to suppress the interference completely.

When lcp_0 *and* lcp_1 are used with front end filtering, lcp_1 performs slightly better than lcp_0 due to more effective spectrum shaping. When no prefiltering is employed, the performances get worse due to pulses' limited interference-rejection capability. It should also be noted that the performances are better in the order of lcp_3, lcp_2, lcp_1 and lcp_0 as expected.

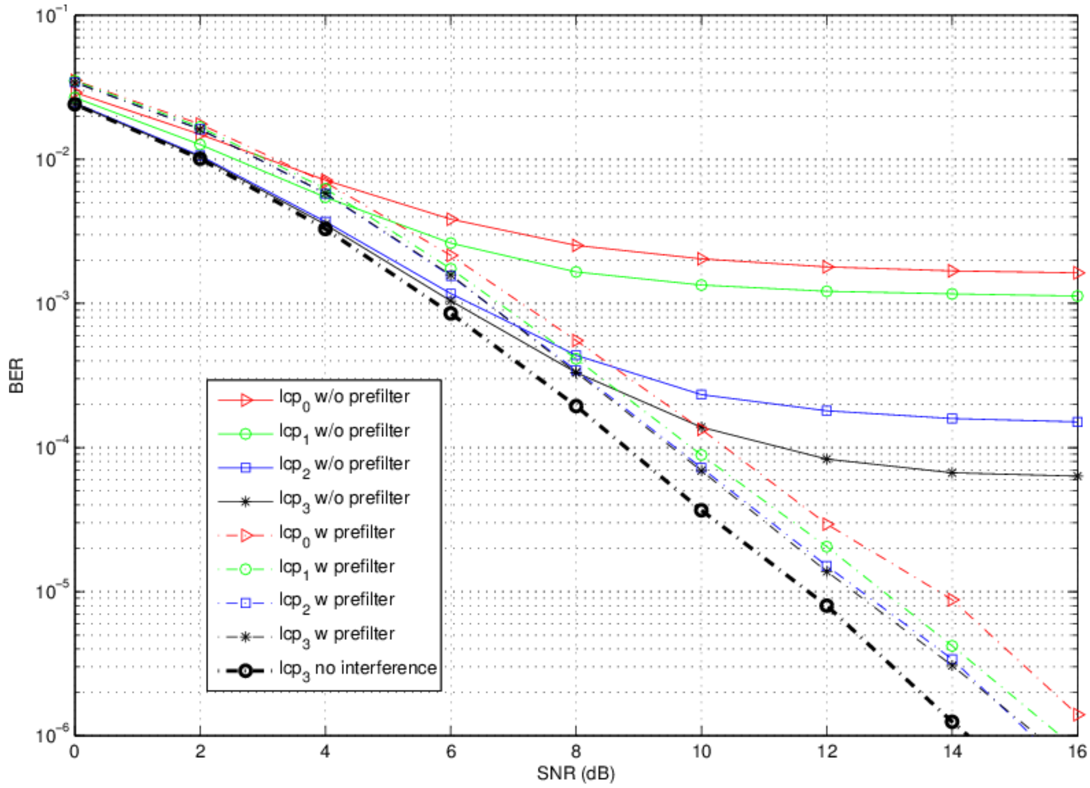

Figure 4.6 : BER performance of a coherent receiver in *CM1* for various SNR values and pulse types.

4.2.2 Noncoherent Receiver

The noncoherent receiver performance of various linearly combined pulses lcp_0, lcp_1, lcp_2 and lcp_3 are assessed in the presence of a wideband interference which has a bandwidth of 20 MHz and 16 subscarriers with the integration time of 16 ns. In Figure 4.7, the BER performances are plotted for various SIR values when SNR = 30dB and 5-tap P-Rake receivers are used.

When there is no prefiltering, the BER performance of the UWB system is poor for all SIR values and all types of linearly combined pulses. All *lcp*'s show similar performances. Using a prefiltering at the front-end, linearly combined pulse improves the BER performance noticeably for lcp_0 and lcp_1, whereas using lcp_2 or lcp_3 with a prefilter at the front-end can suppress the interference independent from the SIR values due to having wider notch width.

In Figure 4.8, the BER performances are plotted for various SNR values when SIR = 0dB and 5-tap P-Rake receivers are used for the same wideband interference.

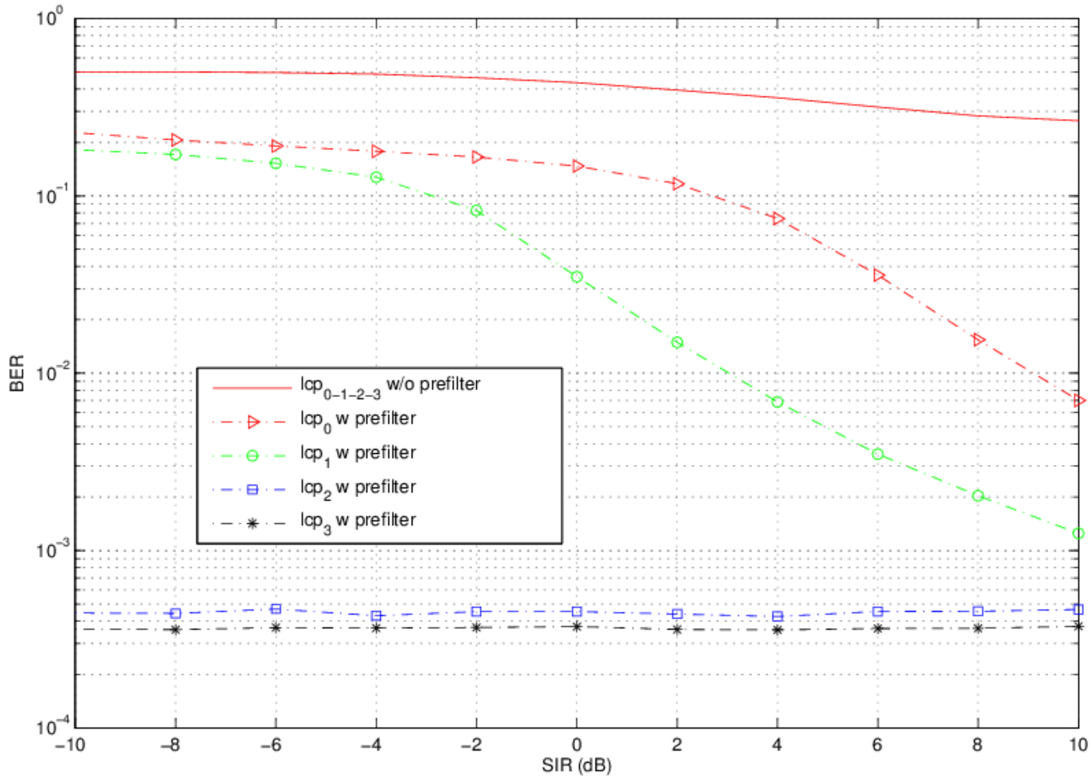

Figure 4.7 : BER performance of a noncoherent receiver in *CM1* for various SIR values and pulse types.

When there is no prefiltering, the BER performance of the UWB system is poor for all SNR values and all types of linearly combined pulses due to integration of noise and interference cross-terms. Using prefiltering at the front-end linearly combined pulse improves the BER performance slightly for a lcp_0 and *lcp1*, whereas using lcp_2 or lcp_3 with a prefilter at the front-end can improve the system performance significantly due to having wider notch width.

4.3 Effects of interference types

In this section, the coherent receiver performances of lcp_1 are assessed in the presence of wideband interference which has various bandwidth values and different number of subcarriers.

4.3.1 Effects of bandwidth

The coherent receiver performance of lcp_1 without prefiltering are assessed in the presence of a wideband interference which has various bandwidths of 5 MHz, 10 MHz and 20 MHz and 256 subcarriers. In Figure 4.9, the BER performances of lcp_1

are plotted for various SIR values when SNR = 15 dB and 5 tap P-Rake receiever are used.

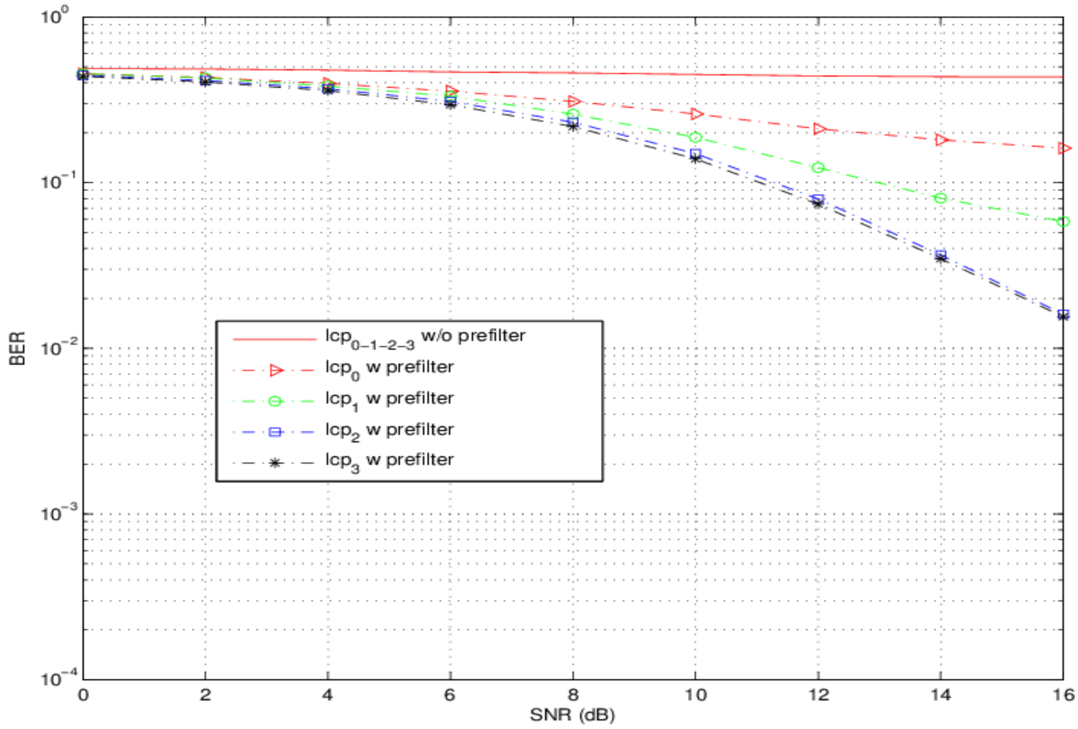

Figure 4.8 : BER performance of a noncoherent receiver in *CM1* for various SNR values and pulse types.

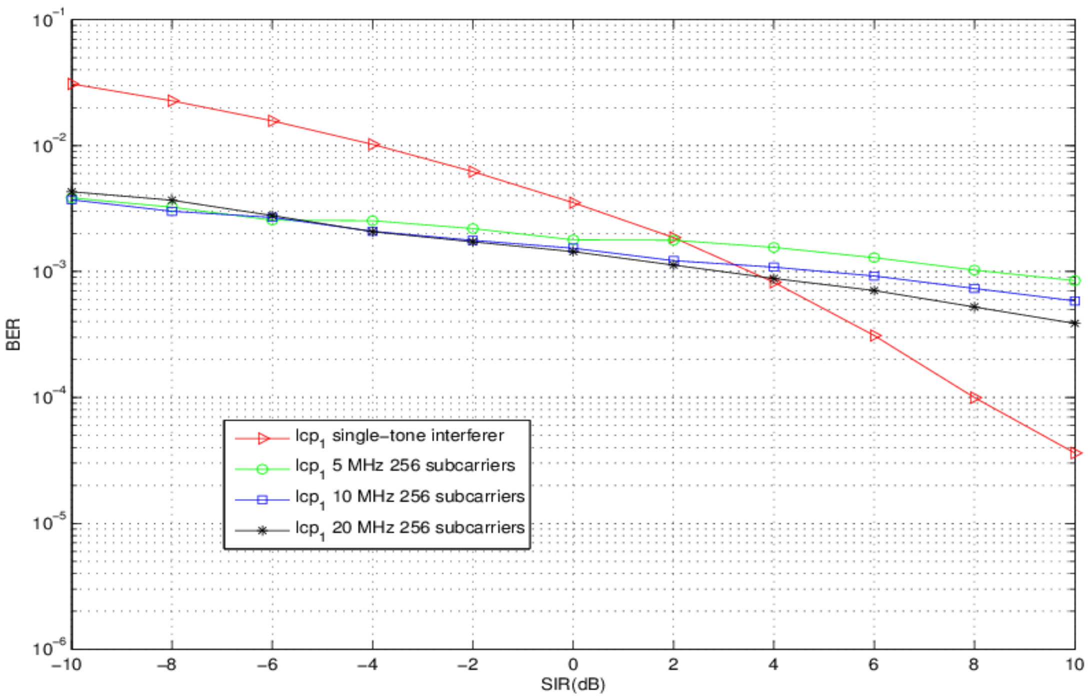

Figure 4.9 : BER performance of a coherent transceiver using lcp_1 in *CM1* for various SIR values and bandwidths.

The performance of lcp_1 with a single-tone interferer when matched filtering employed serves as a benchmark. WiMAX–OFDM employs N = 256 subcarriers which increases the averaging effect and hence the Gaussianity of the interference. It should also be noted that, for the most of the SIR values, the BER tends to decrease as the interferer bandwidth increases. This is because per-subcarrier interference power spectral density decreases as the bandwidth increases, where the average interference power is constant. A similar observation was made in [26], where they analyzed the effect of WiMAX-OFDM interference.

4.3.2 Effects of subcarriers

Finally, the coherent receiver performance of lcp_1 without prefiltering is assessed in the presence of a wideband interference which has various number of subcarriers of 64, 128 and 256, and a bandwidth of 20 MHz. In Figure 4.10, the BER performances are plotted for various SIR values when SNR = 15 dB and 5-tap P-Rake receivers are used.

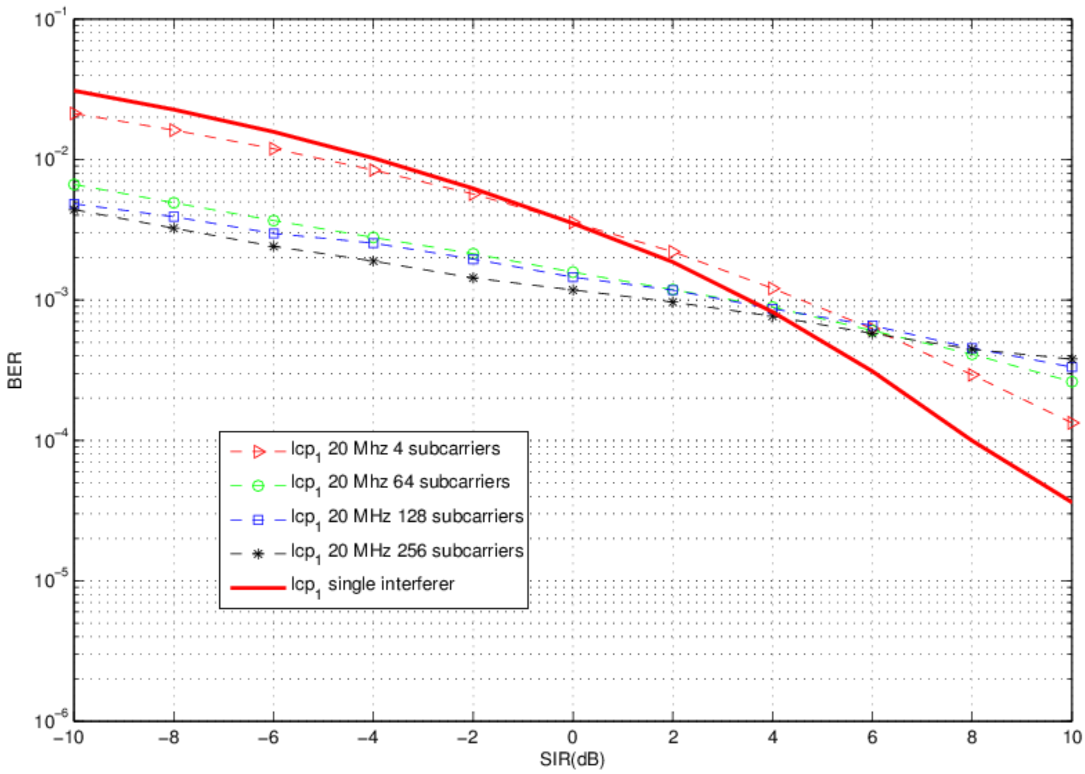

Figure 4.10 : BER performance of a coherent transceiver using lcp_1 in *CM1* for various SIR values and subcarriers.

All subcarriers of the WiMAX-OFDM signal contribute to every time-domain sample of the interference signal, thus there is the averaging effect invoking the Central Limit Theorem. It should be also noted that, for the most of the SIR values, the BER tends to decrease as the number of subcarriers increases. This is because per-subcarrier interference power spectral density decreases as the number of subcarriers increases, where the average interference power is constant.

In this chapter, the performance of an IEEE 802.15.4a based system that can coexist with a narrowband or wideband primary system is investigated considering the realistic implementation issues such as practical receiver types, pulse types and interference types.

5. CONCLUSION AND FUTURE WORK

In this thesis, the various implementations of linear combination of pulses and the corresponding coherent and noncoherent receiver structures are investigated in order for an IEEE 802.15.4a based UWB system operating in the same frequency band with a narrowband or wideband licensed system.

Accordingly, a modified transceiver structure that employs different types of linear combination of pulses allowing coexistence was presented and the system performance was compared with the performance of an IEEE 802.15.4a system implemented according to the standard. Moreover, the effects of wideband system parameters (bandwidth and number of subcarriers) and different linearly combined pulses were considered.

The study showed that using a linearly combined pulse, the BER performances of coherent and noncoherent receiving structures may be slightly degraded when there is no active licensed system (i.e., interferer), however, the performances can be significantly improved with prefiltering at the receiver when a narrowband licensed system is active.

In addition, in the presence of a wideband interference employing other higher order linearly combined pulses (e.g., lcp_2, lcp_3) can better compensate the system performance due to having wider notch and more effective spectrum shaping. Apart from that, it is shown that for a fixed subcarrier with increasing bandwidth; the BER tends to decrease. In addition, increasing the number of subcarriers for a fixed bandwidth has same effects. It can be concluded that the UWB system will best coexist peacefully with a WiMAX system, which has a wider bandwidth and a large number of subcarriers.

The results presented are important as the modified transceiver structure can achieve a reasonable system performance while complying to the European and Japanese regulatory agency mandates.

While this study focused on the performance of the IEEE 802.15.4a based UWB systems in the presence of a single narrowband or a wideband interference, the future work may also include the effects multiple narrowband and wideband active primary systems on the system performance when linear combination of pulses and modified transceiver structures are used.

REFERENCES

[1] Win, M. Z., and Scholtz, R. A. (1998). On the energy capture of ultra-wide bandwidth signals in dense multipath environments, *IEEE Commun. Lett.*, vol. 2, pp. 245-247

[2] Welborn, M. L. (2001). System considerations for ultra-wideband wireless networks, *in Proc. IEEE Radio and Wireless Conf. 2001, Boston, MA, pp. 5-8*

[3] Solimene, R., Soldovieri, F., Prisco, G., Pierri, R. (2009). Three-Dimensional Through-Wall Imaging Under Ambiguous Wall Parameters, *IEEE Transactions on Geoscience and Remote Sensing,* vol.47, no.5, pp. 1310 – 1317

[4] Hjortland, H. A., Lande, T. S.B. (2009). CTBV Integrated Impulse Radio Design for Biomedical Applications, *IEEE Transactions on Biomedical Circuits and Systems*, vol.3, no.2, pp. 79 – 88

[5] Sakkila, L., Tatkeu, C., Boukour, F., El Hillali, Y., Rivenq, A., Rouvean, J. M. (2008). UWB Radar systemforroad anti-collisionapplication, *Proceedings of International Conference on Information and Communication Technologies: From Theory to Applications,* pp. 1-6

[6] Gezici, S., Tian, Z., Giannakis, G. B., Kobayashi, H., Molisch, A. F., Poor, H. V., Sahinoglu, Z. (2005). Localization via Ultra-Wideband Radios, *IEEE Signal Processing Magazine*, pp.70-84

[7] Taylor, J. D. (1995). Introduction to Ultra-Wideband Radar Systems, CRC Press, Boca Raton, Florida

[8] Hussain, M. G. M. (1998). Ultra-wideband impulse radar – An overview of the principles, *IEEE Aerosp. Electron. Syst. Mag., and Wireless Conf.* vol. 13, no.9, pp. 9-14

[9] Federal Communications Commission (2002). First Report andOrder 02-48., Washington, DC

[10] Reed, J. H. et al., (2005). An Introduction to Ultra Wideband Communication Systems, Prentice Hall

[11] Balakrishnan, J., Batra, A., Dabak, A. (2003). A multi-band OFDM systemfor UWB communication. *in Proc. IEEE Conf. Ultra Wideband Systems and Technologies UWBST'03. Reston, VA, pp. 354-358*

[12] ECMA Std. 368 3th Ed. (2008). High Rate Ultra Wideband PHY and MAC Standard

[13] Karapistoli, E., Pavlidou, F. N., Gragopoulos, I., Tsetsinas, I. (2010). Code Shift Keying Modulation For Low-Rate UWB Communications

Under Dense Multipath, *in Proc. IEEE Communications Magazine*, vol. 48, no.1, pp. 47-53

[14] IEEE Std 802.15.4a-2007 (2007). Part 15.4: Wireless Medium Access Control (MAC) and Physical Layer (PHY) Specifications for Low-Rate Wireless Personal Area Networks (WPANs)

[15] European Commission (2009). 2009/343/EC: Commission Decision of 21 April 2009 amending Decision 2007/131/EC on allowing the use of the radio spectrum for equipment using ultra-wideband technology in a harmonized manner in the Community, *Official Journal of European Union.*, L 109, 9-13, Apr. 2009

[16] Wang, Y., Dong X., Fair, I. J. (2007). Spectrum shaping and NBI suppression in UWB Communications, *IEEE Trans. Wireless Commun.*, vol. 6, pp. 1944-1952

[17] Wu, X., Tian, Z., Davidson, T. N., Giannakis, G. B. (2006). Optimal Waveform Design for UWB Radios, *IEEE Transactions on Signal Processing*, vol. 54, no.2, pp. 2009 – 2021

[18] Dotlic, I., Tian Z., Kohno, R. (2007). Optimal Waveform Design for UWB Radios, *IEEE Journal of Selected Topics in Signal Processing*, vol. 1, no.1, pp. 21 – 30

[19] Erküçük, S., Kaleli, B. A. (2009). Linear combination of pulses for coexistence in the IEEE 802.15.4a standard, *IEEE Proc. SIU'09*, pp. 620-623

[20] Zhao, L., Haimovich, A. M. (2002). Performance of ultra-wideband communications in the presence of interference**,** *IEEE Jour. Select. Areas Commun.*, vol. 20, pp. 1684-1690

[21] Hamalainen, M., Hovinen, V., Tesi, R., Iianatti, J. H. J., Latva-aho, M. (2002). On the UWB system coexistence with GSM900, UMTS/WCDMA, and GPS, *IEEE Jour. Select Areas Commun.*, vol. 20, pp. 1712-1721

[22] Di Renzo, M., Tempesta, F., Annoni, L. A., Santucci, F., Graziosi, F., Minutolo, R. and Montanari, M. (2009).Performance evaluation of IR-UWB D-Rake receivers over IEEE 802.15.4a multipath fading channels with narrow-band interference.**,** *IEEE Proc. ICUWB'09,* pp. 71-76

[23] Cui, S., Teh, K. C., Li, K. H., Guan, Y.L, and Law, C. L., (2007). Narrowband interference suppression in transmitted reference UWB systems with inter-pulse interference, *IEEE Proc. ICUWB'07.*, pp. 895-898

[24] Wu, X. L., Sha, X. J., Li, C., Zhang, N. T. (2010). Pulse Shaping for Cognitive Ultra-Wideband Communications, *Proceedings of Wireless Communications and Mobile Computing*, pp. 772-786

[25] Erküçük, S., Kim, D. I., Kwak, K. S. (2006). Code Shift Keying Modulation For Low-Rate UWB Communications Under Dense Multipath, *in Proc. IEEE Global Telecommunications Conference GLOBECOM'06*, pp. 1-5

[26] Snow, C., Lampe, L., Schober, R. (2009). Impact of WiMAX Interference on MB-OFDM UWB Systems: Analysis and Mitigation, IEEE Transactions on Communications, vol. 57, no.9, pp. 2818 – 2897

[27] Molisch, A. F., Foerster, J. R., Pendergrass, M. (2003).Channel Models for Ultra-wideband Personal Area Networks, *IEEE Wireless Communications*, vol.10, pp. 14-21

[28] Win, M. Z., and Scholtz, R. A.(1998). On the robustness of ultra-wide bandwidth signals in dense multipath environments, *IEEE Commun. Lett.*, vol. 2, no.2, pp. 53-55

[29] Cassioli, D., Win, M. Z., Molisch, A. F. (2002**).** A statistical model for the UWB Indoor Channel, *IEEE J. Select Areas Comm*., vol. 20, pp. 1247 – 1257

[30] Hashemi, H. (1993). Impulse response modeling of Indoor Radio Propagation Channels, *IEEE J. Select Areas Comm., vol. 11, no.7, pp. 967 – 978*

[31] Foerst, J. (2002). Path Loss Proposed Text and S-V Model Information, *Intel Research and Dev.*

[32] Yang, H. (2003). UWB Channel Modelling, *Journal of Korean Institute of Communication and Science Telecommunications*, vol.20, no.2, pp. 42-52

[33] Molisch, A. F. (2005). UWB Propagation channels., Book chapter 1, pp.1

[34]Molisch, A. F. et. al. (2005). IEEE 802.15.4a channel model – final report., Tech. Rep. Document IEEE 802.15-04-0662-02-004a

[35] Fındıklı, Ç., Erküçük, S. (2010). Effects of channel models and optional data rates on the IEEE 802.15.4a system performance, *IEEE Proc. SIU’10*, pp. 25-28

[36] Shin, C. K., Kim, S. H., Yang, Q., Zhang, W., Kwak, K. S. (2006). Performance Comparison of TH-BPPM/TH-BPSK using Rake Receivers in IEEE 802.15.4a Channel Model, *International Symposium on Communications and Information Technologies, ISCIT '06.*, pp. 1025-1030

[37] Molisch, A. F. et. al. (2003). An efficient low-cost time-hopping impulse radio for high data rate transmission, *in Proc. IEEE 6th International Symposium on Wireless Personal Multimedia Communications WPMC’03*

[38] Choi, D. J., Stark, W. E. (2002).Performance of ultra-wideband communications with suboptimal receivers in multipath channels., *IEEE Journal of Selected Areas Comm.*, vol. 20, no. 9pp. 1754-1766

[39] Cassioli, D., Win, M. Z., Vatalaro, F., and Molisch, A. F. (2003). Performance of low-complexity Rake reception in a realistic UWB channel., *in Proc. IEEE International Conference on Commun. ICC’03.,*vol.2,pp. 763-767

[40] Rajwani, F., Beaulieu, N. C. (2005). Simplified bit error rate analysis of PAPM-UWB with MRC and EGC in lognormal fading channel, *in Proc. IEEE International Conference on Communications ICC'03.,*vol. 5, pp. 2886-2889

[41] Foerster, J. R. (2001). The effects of multipath interference on the performance of UWB systems in an indoor wireless channel, *in Proc. IEEE Vehicular Technology Conference on Commun. VTC'03.,*pp. 1176-1180

[42] Maali, A., Mesloub, A., Djeddou, M., Mimoun, H., Baudoin, G., Ouldali, A. (2009). Adaptive CA-CFAR Threshold for Non-Coherent IR-UWB Energy Detector Receivers, *IEEE Communications Letters*, vol.13, no.12, pp. 959 – 961

[43] Thomas, W. P., McClellan, J. H. (1972). Chebyshev Approximation for Nonrecursive Digital Filters with Linear Phase, *IEEE Transactions on Circuit Theory*, vol. CT-19, no.2, pp. 189 – 194

[44] Qiu, R., Lu, I.–T (1996). Wideband wireless multipath channel modeling with path frequency dependence., *in Proc. IEEE International Conference on Commun. ICC'96.*vol. 1, no.1, pp. 277 - 281

[45] Qiu, R., Lu, I. –T (1999).Multipath resolving with frequency dependence for broadband wireless channel modeling., *in Proc. IEEE Trans. Veh. Tech.,* vol. 48, no.1, pp. 273 - 285

[46] Rappaport, T. S. (2002) Wireless Communications: Principles and Practice (2nd ed.), Prentice Hall PTR, Upper Saddle River, NJ

[47]Saleh, A., Valenzuela, R. (1987). A statistical model for indoor multipath propagation., *IEEE Journal on Select. Areas Commun.,* vol.SAC-5, no.2, pp. 128-137

APPENDICES

APPENDIX A: UWB Channel Parameters

Parameters that provide the UWB channel modeling are presented in this section.

A.1 Path Loss and Shadowing

The large-scale channel modeling involves modeling the signal attenuation with distance and is generally referred to as path loss. The path loss in a narrowband system is conventionally defined as,

$$PL(d) = \frac{E\{P_{RX}(d,f_c)\}}{P_{TX}} \quad \textbf{(A.1)}$$

where P_{TX} and P_{RX} are transmit and receive power, respectively, d is the distance between transmitter ad receive, $\mathrm{f_c}$ is the center frequency and the expectation $E\{\}$ is taken over an area that is large enough to allow averaging out of shadowing as well as the small-scale fading. Due to frequency dependence of propagation effects in a UWB channel, the wideband path loss is a function of frequency as well as of distance. It thus makes sense to define a frequency-dependent path loss as [34],

$$PL(d,f) = E\{\int_{f-\frac{\Delta f}{2}}^{f+\frac{\Delta f}{2}} \left|H(\tilde{f},d)\right|^2 d\tilde{f}\} \quad \textbf{(A.2)}$$

where $\left|H(\tilde{f},d)\right|$ the transfer is function from transmitting antenna connector to the receiving antenna connector, and Δf is chosen small enough so that diffraction coefficients, dielectric constants, etc., can be considered constant within that bandwidth.

The total path loss is obtained by integrating over the whole bandwidth of interest.

It is assumed that the path loss as a function of frequency and distance can be written as product of the terms [34]

$$PL(d,f) = PL(f)PL(d) \quad \textbf{(A.3)}$$

The frequency dependence of the path loss is given as [44][45]

$$\sqrt{PL(f)} \propto f^{-\kappa} \quad \textbf{\textit{(A.4)}}$$

where κ is the frequency dependence factor. The distance dependence of the path loss in dB is described by [34]

$$PL(d) = PL_o + 10n\log_{10}\left(\frac{d}{d_o}\right) + S \quad \textbf{(A.5)}$$

Where S accounts for shadowing and is a Gaussian distributed random variable with zero mean and the standard deviation σ_s.

A.2 Power Delay Profile

Power delay profile relates the power of the received signal with the delay experienced by the multipath component and is defined as the square magnitudes of the impulse response of the signal averaged over a local area as [46],

$$PDP(\tau) = |h(t,\tau)|^2 \quad \textbf{(A.6)}$$

The impulse response in complex baseband is based on the Saleh-Valenzuela model which is given in general as [47]

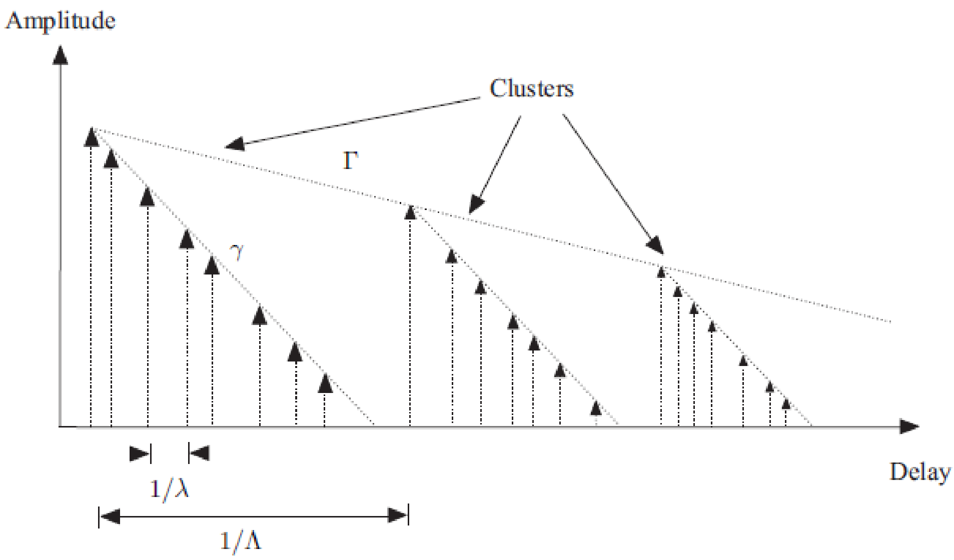

Figure A.1 : Principle of Saleh-Valenzuela model[44].

$$h_{discr}(t) = \sum_{l=0}^{L-1}\sum_{k=0}^{K-1}\alpha_{k,l}\,exp(j\varphi_{k,l})\delta(t - T_l - \tau_{k,l}) \quad \textbf{(A.7)}$$

Where $\alpha_{k,l}$the tap weight of the kth component in the lth cluster is T_l is the arrival time of the l^{th} cluster and $\tau_{k,l}$ is the delay of the k^{th} multipath component relative to the l^{th} cluster arrival time T_l. The phases $\varphi_{k,l}$ are uniformly distributed for a bandpass system, the phase is taken as a uniformly random variable in the range from [0,2π] [34]

The number of clusters L is an important parameter of the model and is assumed to be Poisson-distributed [34]

$$pdf_L(L) = \frac{(\bar{L})^L \, exp(-\bar{L})}{L!} \tag{A.8}$$

so that the mean $\bar{L}$ completely characterizes the distribution.

The distribution of cluster arrival times are given by a Poisson process

$$p(T_L|T_{L-1}) = -\Lambda_l exp[-\Lambda_l(T_L - T_{L-1})],\ l > 0 \tag{A.9}$$

where $-\Lambda_l$ is the cluster arrival rate.

The ray arrival times are modeled with mixtures of two Poisson process as follows

$$p(\tau_{k,l}|\tau_{(k-1),l}) = \beta\,\lambda_1 \exp[-\lambda_1(\tau_{k,l} - \tau_{(k-1),l})]$$

$$+(\beta - 1)\,\lambda_2 \exp[-\lambda_2(\tau_{k,l} - \tau_{(k-1),l})],\ k > 0 \tag{A.10}$$

Where β is the mixture probability, while $\lambda_1$and λ_2 are the ray arrival rates.

For some environments, most notably the industrial environment, a dense arrival of multipath components was observed, such as each resolvable delay bin contains significant energy. In that case, the concept of arrival rates losses its meaning, and a realization of the impulse response based on a tapped delay line model with regular tap spacing is to be used.

The power delay profile (the mean power of different paths) is exponential within each cluster [34]

$$E\left\{\left|\alpha_{k,l}\right|^2\right\} = \ \Omega_l \frac{1}{\gamma_l[(1-\beta)\lambda_1 + \beta\lambda_2 + 1]} \exp(-\tau_{k,l}/\gamma_l) \tag{A.11}$$

Where $\Omega_l$the integrated energy of the l^{th} is cluster and γ_l is the inta-cluster decay time constant.

Further, the mean over cluster-shadowing mean over small-scale fading energy normalized to γ_l of the l^{th} cluster follows in general exponential decay.

$$10\ log_{10}(\Omega_l) = 10 log(exp(-T_l/\Gamma)) + M_{cluster} \tag{A.12}$$

Where $M_{cluster}$ is normally distributed random variable with standard deviation $\sigma_{cluster}$ around it.

Finally, the cluster decay rates are found to depend linearly on the arrival time of the cluster

$$\gamma_l = k_\gamma T_l + \gamma_o \quad \textbf{(A.13)}$$

where k_γ describes the incrase of the decay constant with delay.

In this model, particularly for some NLOS scenarios (office and industrial), the shape of the power delay profile can be different, namely on a log-linear scale.

$$E\left\{\left|\alpha_{k,l}\right|^2\right\} = \left(1 - \chi \exp\left(\frac{-\tau_{k,l}}{\gamma_{rise}}\right)\right) \exp\left(\frac{-\tau_{k,l}}{\gamma_1}\right) . \frac{\gamma_1 + \gamma_{rise}}{\gamma_1} \frac{\Omega_1}{\gamma_1 + \gamma_{rise}(1-\chi)} \quad \textbf{(A.14)}$$

where the parameter χ describes the attenuation of the first component, the parameter γ_{rise} determines how fast the power delay profile incrases to its local maximum, and γ_1 determines the decay at late times.

A.3 Delay Dispersion

Delay dispersion is defined to occur when the channel impulse response lasts for a finite amount of time or channel is frequency selective [33]. Delay dispersion in multipath channel is characterized by two important parameters, mean excess delay and root mean square delay spread.

Excess delay is the relative delay of k^{th} received multipath component as compared to the first arriving path, and is denoted as τ_k. Mean excess delay is defined as the first moment of the power delay profile given by [34],

$$\tau_m = \frac{\int_{-\infty}^{\infty} PDP(\tau)\tau d\tau}{\int_{-\infty}^{\infty} PDP(\tau) d\tau} \quad \textbf{(A.15)}$$

The root mean square delay is defined as the second central moment of the power delay profile given by,

$$\tau_{rms} = \left(\frac{\int_{-\infty}^{\infty} PDP(\tau)\tau^2 d\tau}{\int_{-\infty}^{\infty} PDP(\tau) d\tau} - \left(\frac{\int_{-\infty}^{\infty} PDP(\tau)\tau d\tau}{\int_{-\infty}^{\infty} PDP(\tau) d\tau}\right)^2\right)^{\frac{1}{2}} \quad \textbf{(A.16)}$$

The delay spread depends on the distance, however this effect is neglected in the channel model for simplicity [34].

A.4 Smale Scale Fading

The rapid fluctuations of the received signal strength over very short travel distance of few wavelengths or short time durations on the order of seconds are called small-scale fading. In this model, the distribution of small scale amplitudes is Nakagami

$$pdf(x) = \frac{2}{\Gamma(m)}\left(\frac{m}{\Omega}\right)^{m} x^{2m-1}\, exp\left(-\frac{m}{\Omega}x^2\right) \qquad \textbf{(A.17)}$$

Where $m \geq 1/2$ is the Nakagami m-factor, $\Gamma(m)$ is the gamma function and Ω is the mean-square value of the amplitude. The m-parameter is modeled as a lognormally distributed random variable, logarithm of which has a mean μ_m and standard deviation σ_m. Both of these values can have a delay dependence [34],

$$\mu_m(\tau) = m_o - k_m\tau \qquad \textbf{(A.18)}$$

$$\sigma_m = \hat{m}_o - \hat{k}_m\tau \qquad \textbf{(A.19)}$$

For the first component of each cluster, the Nakagami factor is assumed to be deterministic and independent of delay [34]

$$m = \tilde{m}_o \qquad \textbf{(A.20)}$$

CURRICULUM VITAE

Name Surname: Çağlar FINDIKLI

Place and Date of Birth: Ankara, 05/01/1988

Address: Küçüksu Mah. ÖztürkSok. 2001 Sitesi J Blok No:7 Çengelköy / İST

E-Mail: caglarfkhas@hotmail.com

B.Sc.: Kadir Has University, Electronics Engineering 2009

Professional Experience and Rewards:

March 2012 – present	Huawei Turkey R&D Center Istanbul, TURKEY Assistant Software Test Engineer
March 2011 – March 2012	NETAŞ Telecommunications Inc. Istanbul, TURKEY TÜBİTAK TEYDEB Project Expert Through Wall Imaging with Ultra-wideband Radar
November 2010 – July 2011	EuropeanUnion 7th Framework Research Programme Project Researcher Coexistence of Ultra-Wideband and Licensed Systems

List of Publications and Patents:

- Fındıklı, Ç., Erküçük, S., 2010: Effects of Channel Models and Optional Data Rates on the IEEE 802.15.4a System Performance (InTurkish). *Proceedings of 18th Signal Processing and Communication Applications Conf. SİU'10,* 22-24 April 2010, Diyarbakır, Turkey.

PUBLICATIONS/PRESENTATIONS ON THE THESIS

- Fındıklı, Ç., Erküçük, S., Çelebi, M.E., 2011: Performance of IEEE 802.15.4a Systems in the Presence of Narrowband Interference. *Proceedings of International Conference on Ultra-wideband, ICUWB 2011,* 14-16 September 2011, Bologna, Italy.